

ST 124-M

5/26/69

A DESCRIPTION OF THE ST 124-M
INERTIAL STABILIZED PLATFORM
AND ITS APPLICATION TO THE
SATURN V LAUNCH VEHICLE



Eclipse-Pioneer Division
TETERBORO, N. J.



III.6
XIV.1

A DESCRIPTION OF THE ST124-M
INERTIAL STABILIZED PLATFORM AND ITS
APPLICATION TO THE SATURN V
LAUNCH VEHICLE

7511 - 64 - R11

May 26, 1964

Prepared by: B. J. O'Connor
B. J. O'Connor

THE BENDIX CORPORATION
ECLIPSE-PIONEER DIVISION
TETERBORO, NEW JERSEY

FOREWORD

This report is a description of the ST124-M inertial stabilized platform system and its application to the Saturn V launch vehicle. It is a summary report providing the system concept, and not a theoretical presentation.

Mathematical equations were included only where necessary to describe the equipment; however, the detail derivations supporting these equations were not presented since this was not the theme of the paper.

APPROVAL

A DESCRIPTION OF THE ST124-M INERTIAL
STABILIZED PLATFORM AND ITS APPLICATION TO THE
SATURN V LAUNCH VEHICLE

by

B. J. O'CONNOR

The information in this report has been reviewed for security classification. Review of any information concerning Department of Defense or Atomic Energy Commission programs has been made by the MSFC Security Classification Officer. The highest classification has been determined to be Unclassified.

ACKNOWLEDGEMENT

The writer would like to acknowledge the technical assistance given by C. Mandel, Chief, and H. Thomason, Deputy Chief, of the Inertial Sensors and Stabilizers Division, Astrionics Laboratory of the George C. Marshall Space Flight Center, Huntsville, Alabama.

TABLE OF CONTENTS

SECTION	DESCRIPTION	PAGE
1.0	Introduction	1
2.0	A System Description of the ST124-M	4
2.1	The Platform Configuration	4
2.2	The Platform Servo System	12
2.3	The Gimbal Sensors	14
2.4	The Erection System	23
2.5	The Azimuth Laying System	25
2.6	The ST124-M System Block Diagram	28
3.0	The Inertial Components	32
3.1	The AB5-K8 Stabilizing Gyro	32
3.2	The AB3-K8 Pendulous Gyro Accelerometer	36
4.0	The Single Axis Servo Loop	41
5.0	The Platform Characteristic Equation	47
6.0	The Coning or Rectification Drift of a Three Gimbal Platform	57
7.0	A Physical Description of the ST124-M Platform	59
8.0	The Platform Servo Assembly	67
9.0	The AC Power Supply	72
	Bibliography	73

LIST OF ILLUSTRATIONS

FIGURE	TITLE	PAGE
1	Inertial Stabilized Platform System Saturn V and IB	2
2	Inner Gimbal Gyro Orientation	4
3	Inner Gimbal Accelerometer Orientation	6
4	The Launch Configuration of the Three Gimbal Platform	7
5	The Launch Configuration of the Four Gimbal Platform	9
6	ST124-M Gimbal Configuration	10
7	Platform Pivot Configuration	11
8	Block Diagram of Platform Gimbal Servo Loop	13
9	Schematic Block Diagram of Pivot Multi-Speed Resolver Digital Encoder	15
10	Resolver Chain ST124-M Mod III	18
11	Definition of Prime and Double Prime Spaces	19
12	Resolver Chain Output Block Diagram	22
13	Gas Bearing Pendulum	24
14	Erection System Block Diagram	26
15	Inner Gimbal Laying System Schematic	27
16	Azimuth Alignment Block Diagram	29
17	Guidance System Interconnection Block Diagram	30
18	Saturn AB5-K8 Gyro Assembly	33
19	Saturn AB5-K8 Inner Cylinder Assembly	34
20	Saturn AB5-K8 Gas Bearing Assembly	34
21	AB5-K8 Gyro Assembly	34
22	AB3-K8 Schematic	36
23	AB3-K8 Integrating Gyro Assembly	38
24	Single Axis Block Diagram	41
25	ST124-M X or Y Gyro Loop Phase Modulus Plot	45

LIST OF ILLUSTRATIONS
(Continued)

FIGURE	TITLE	PAGE
26	ST124-M X or Y Gyro Servo Amplifier Frequency Response	46
27	ST124-M Signal Flow Diagram for a Three Gimbal Platform	48
28	Damping Ratio (ξ) Versus ϕ_X for the Characteristic Equation $\left[\Delta \ Y \right]$	54
29	Damping Ratio (ξ) Versus ϕ_X for the Characteristic Equation $\left[\Delta \ Y \text{ Secant} \right]$	56
30	ST124-M Three Gimbal Platform	60
31	ST124-M Four Gimbal Platform	61
32	Inner, Middle and Outer Gimbal	62
33	Redundant Gimbal and Frame	62
34	ST-124 with Covers Removed	65
35	Fixed and Movable Prism	66
36	Servo Amplifier Card	69
37	Torquer Power Stage	69
38	Gimbal Servo Loop	70
39	Platform Servo Amplifier Assembly	71

SECTION 1.0

INTRODUCTION

The ST124-M inertial platform system will provide the inertial reference coordinates, thrust velocity and vehicle attitude measurements with respect to these coordinates, for guidance and control of the Saturn IB and Saturn V space boosters.

Three ST124-2 production prototype systems have successfully flown as passengers on vehicles SA-3, 4, and 5 of the Saturn I program. On May 28, 1964, a fourth system flew closed loop, providing the second stage cutoff signal, lateral and pitch steering, as well as attitude control in all three axis. The system took control of vehicle SA-6, of the Saturn I program, 14 seconds after second stage ignition and successfully guided the second stage to cutoff, meeting or surpassing all test objectives.

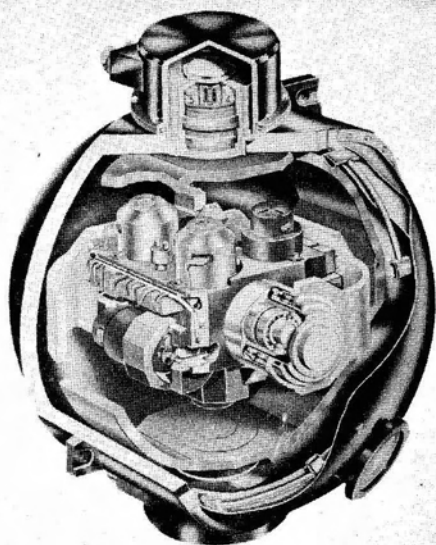
Flight certification of the system was accomplished by ground sled testing at the USAF test track at Holloman, New Mexico. The system was successfully tested with an 8g thrust level and a 20g vibration environment.

The ST124-M system consists of four major assemblies shown in Figure 1. These are

- a. The ST124-M Stable Platform
- b. The Platform Servo Amplifier
- c. The A.C. Power Supply
- d. The Accelerometer Signal Conditioner.

The ST124-M stable platform is designed so that it can be built as as three or four gimbal platform depending on the requirements of the mission profile. The three inner most gimbals of both platform

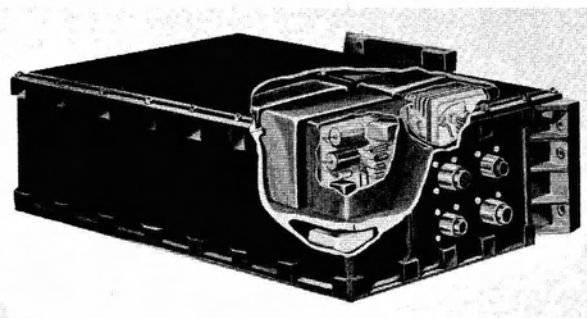
FIGURE 1 INERTIAL STABILIZED PLATFORM SYSTEM SATURN V & IB



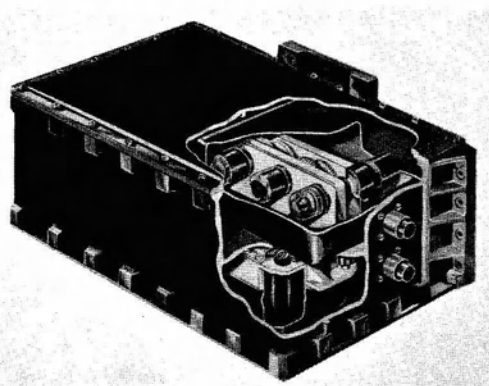
ST-124 M STABLE PLATFORM

SYSTEM FUNCTIONS

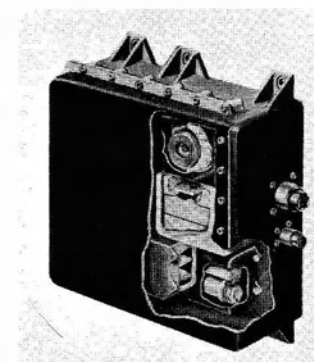
- A. Accelerometer Sensing and Reference.
- B. Vehicle Attitude and Programming.
- C. Guidance Reference Coordinates.



PLATFORM SERVO AMPLIFIER



**ACCELEROMETER SIGNAL
CONDITIONER**



AC POWER SUPPLY

THE GENERAL CORPORATION

THE GENERAL CORPORATION

configurations are identical, thus except for a change in mounting requirements, the two platforms are nearly identical from an electrical interface and system view point. The inner gimbal of the platform is stabilized by three single degree of freedom AB5-K8 gas bearing gyros and carries three AB3-K8 gas bearing pendulous gyro accelerometers which measure the thrust velocity of the booster. The gimbal pivots contain multi-speed resolvers which are used as digital encoders to measure vehicle attitude. An analogue resolver chain is also mounted on the gimbal pivots which provides attitude steering error signals in pitch roll and yaw. This system is a backup system for the digital encoders.

The platform servo amplifier contains the solid state electronics to close the platform gimbal servo loops, the accelerometer servo loops, and an impulse function generator for automatic checkout of each servo loop.

The AC power supply assembly provides the power required for all gyro wheels, the excitation voltage for the servo loops, and the excitation for the resolver chain.

The accelerometer signal conditioner accepts the signals from the accelerometer incremental encoders and shapes them before they are transmitted to the digital computer.

The above named assemblies form the airborne portion of the ST124-M inertial platform system.

SECTION 2.0

A SYSTEM DESCRIPTION OF THE ST124-M

2.1 THE PLATFORM CONFIGURATION

The inner gimbal of the stable platform provides a rotationally fixed body upon which are mounted three accelerometers. Three single degree of freedom AB5-K8 gyros have their input axis aligned along an orthogonal coordinate system \bar{i}_{XA} , \bar{i}_{YA} , \bar{i}_{ZA} of the inner gimbal as shown in Figure 2.

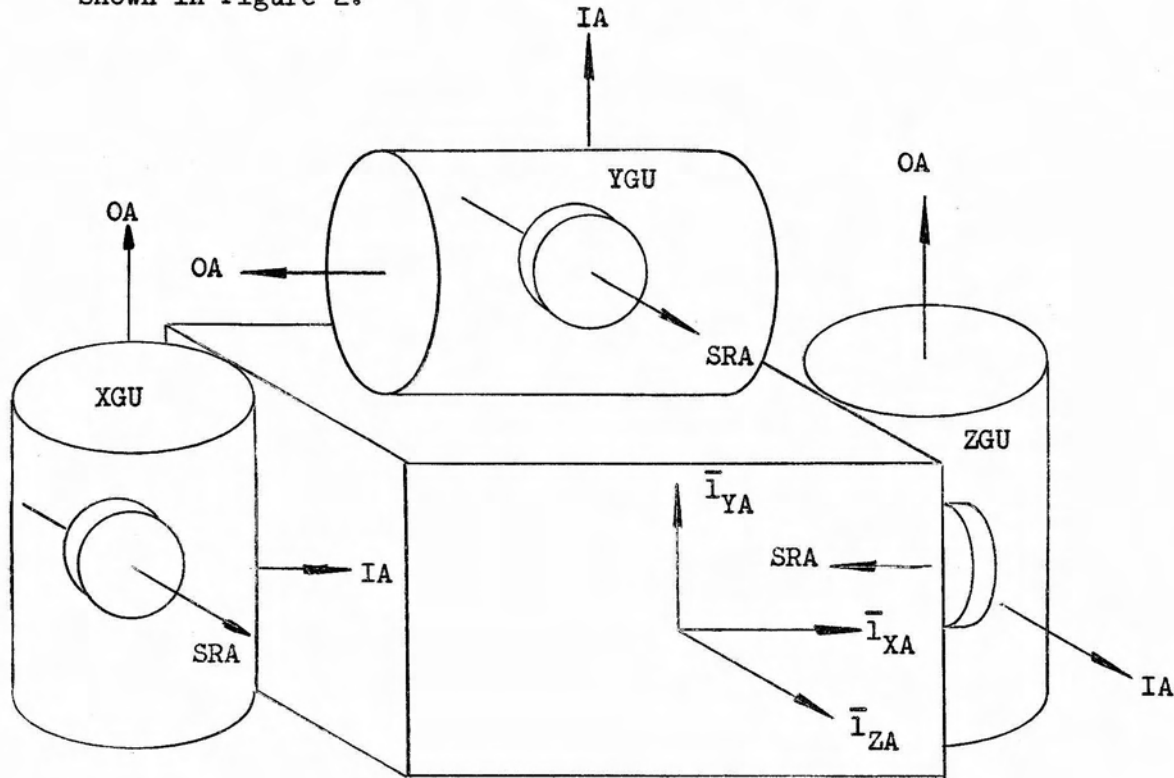


FIGURE 2

INNER GIMBAL GYRO ORIENTATION

The electrical signals from each gyro are fed to the appropriate gimbal torquers to maintain the inner gimbal rotationally fixed in space.

The three AB3-K8 pendulous gyro accelerometers have their input axis aligned along the orthogonal coordinate system \bar{l}_{XA} , \bar{l}_{YA} , \bar{l}_{ZA} of the inner gimbal as shown in Figure 3.

The measuring head contains the pendulous single degree of freedom gyro and the position of the measuring head relative to the case is a measure of thrust velocity along the input axis of each accelerometer.

Assume that the platform erection system will align the \bar{l}_{YA} vector along the launch local vertical and point outward from the earth's surface. The laying system will position the inner gimbal in azimuth so that the \bar{l}_{XA} vector will point down range and the plane formed by the \bar{l}_{XA} , \bar{l}_{YA} vectors will be parallel to the desired thrust flight plane.

The Z accelerometer which is perpendicular to the thrust plane will provide lateral or cross track guidance. The X and Y accelerometers will control the pitch attitude of the thrust vector and also compute the required cutoff velocity.

If the Z accelerometer were ideal, the guidance system will control the thrust vector so it will lie in the \bar{l}_{XA} , \bar{l}_{YA} plane of the inner gimbal. Since the output axis of each gyro also lies in the \bar{l}_{XA} , \bar{l}_{YA} plane as shown in Figure 2, the g^2 or anisoelastic drift of each gyro is negligible.

The configuration of the three gimbal platform on the launch pad is shown in Figure 4. A prism gimbal is mounted to the inner gimbal and is free to rotate about the \bar{l}_{YA} vector of the inner gimbal. The inner gimbal carries its inertial components as shown in Figures 2 and 3, and the Z pivot which couples the inner gimbal to the middle gimbal is along

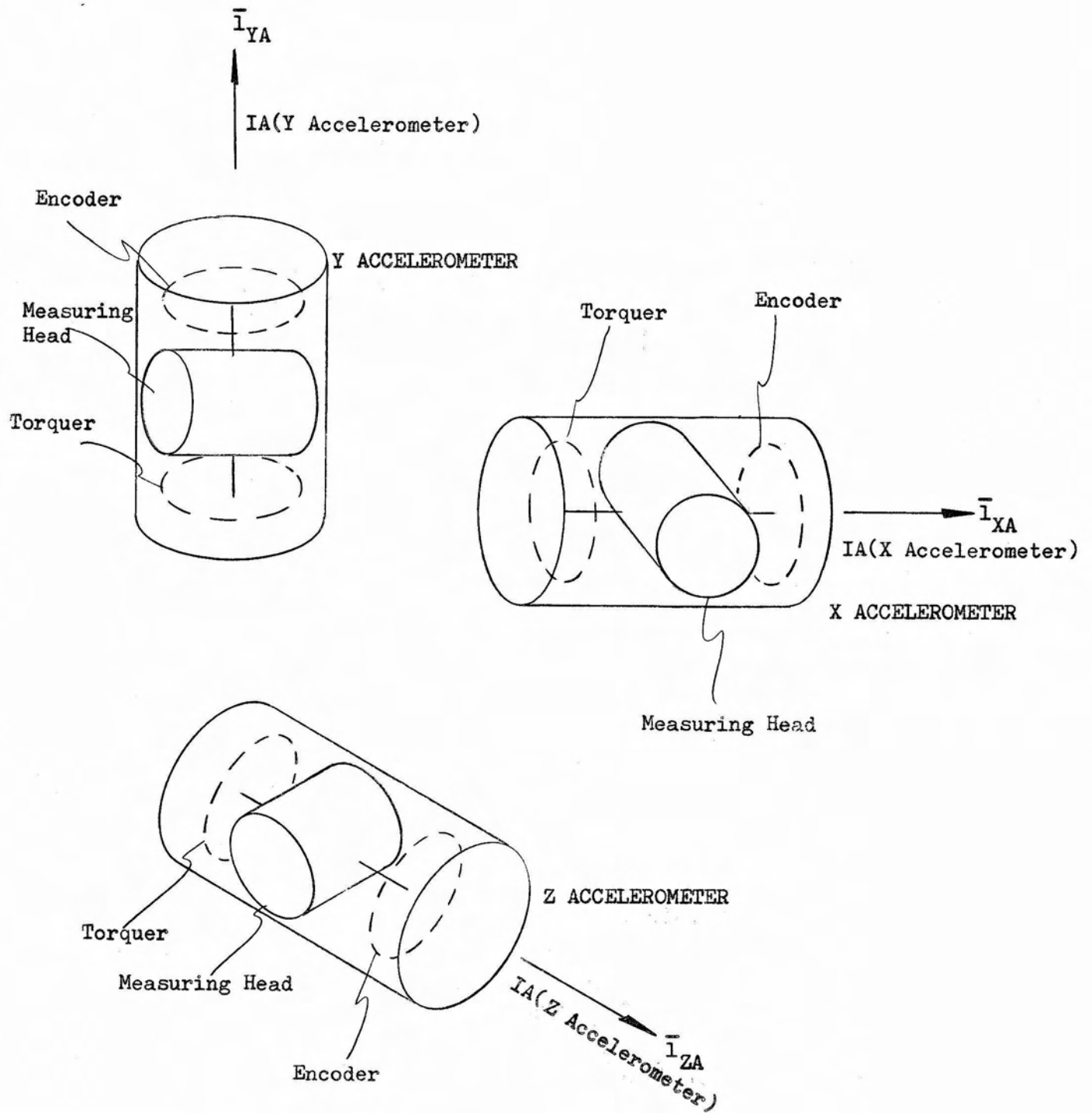


FIGURE 3
INNER GIMBAL ACCELEROMETER
ORIENTATION

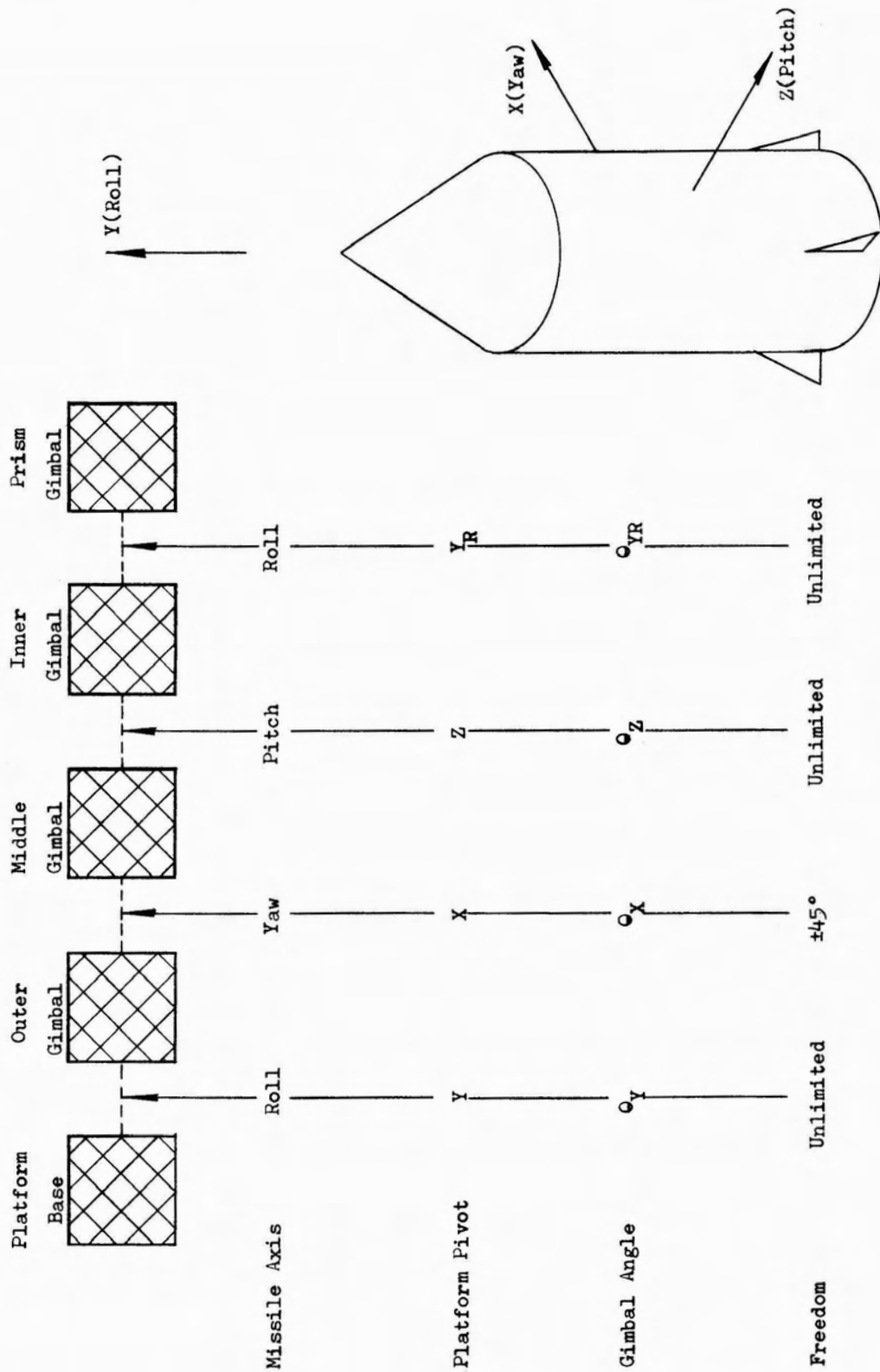


FIGURE 4
THE LAUNCH CONFIGURATION OF THE THREE
GIMBAL PLATFORM

the pitch axis. The X pivot coupling the middle gimbal to the outer gimbal is along the yaw axis and the Y pivot mounting the outer gimbal to the frame is along the roll axis. The three single degree of freedom gyros control torquers on these pivots.

The configuration of the four gimbal platform on the launch pad is shown in Figure 5. It is quite similar to the three gimbal structure with the addition of the redundant gimbal and the X_R pivot. The redundant gimbal is controlled by a time program or an angular sensor on the X pivot. Since the three and four gimbal platforms are almost identical and so not to be repetitious the remainder of the discussion will be concerned with the three gimbal platform. A conventional schematic of the three gimbal platform before launch is also shown in Figure 6.

The platform pivot configuration is shown in Figure 7. The X, Y, and Z pivots are driven by direct drive D.C. torque motors with the Y pivot having twice the torque capacity as the X and Z pivots to accommodate the reflected torque from the X pivot when Θ_X is 45 degrees.

The current transfer for signals across the pivots are slip rings on the Y and Z pivot, and a flex cable joint on the limited motion X pivot. A single speed, multi-speed 32:1 resolver is used as a digital shaft encoder on the X, Y and Z pivots. The analogue resolver chain (1.6 and 1.92KC excitation) has a single speed active unit on all three pivots and locked dummy unit on the X and Y pivots. To facilitate ground checkout and test, the X, Y and Z pivots have a single speed 400 cps resolver.

The Y_R prism gimbal pivot is driven by a 2 \emptyset 400 cps servo motor mounted on the inner gimbal through a gear reduction of 100,000:1. The angle between the prism gimbal and the inner gimbal is accurately sensed by a 25:1 multi-speed synchro. A microsyn is also mounted on the Y_R pivot for initial alignment of the prism gimbal to the inner gimbal during acquisition of the movable prism.

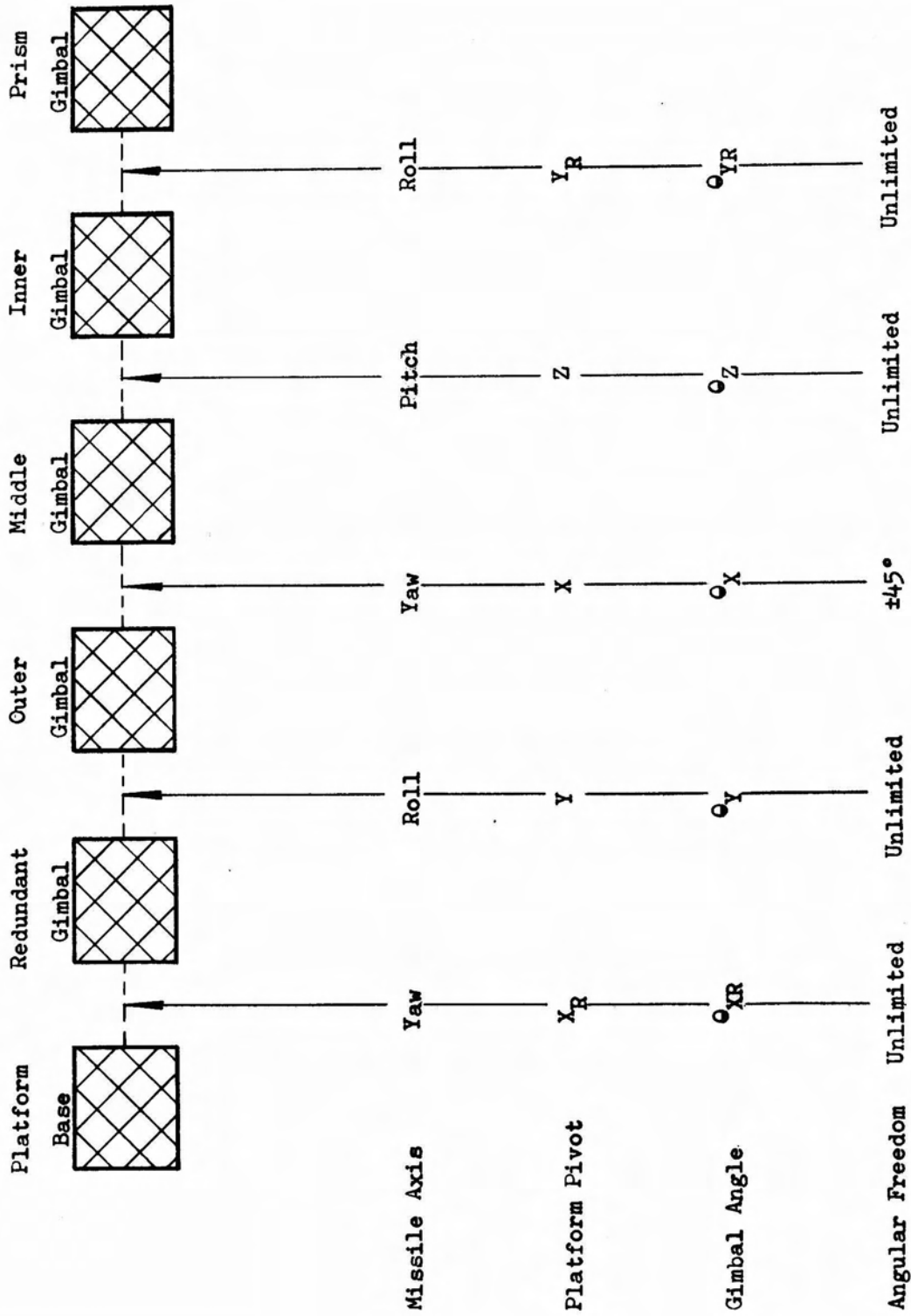


FIGURE 5
THE LAUNCH CONFIGURATION OF THE FOUR
GIMBAL PLATFORM

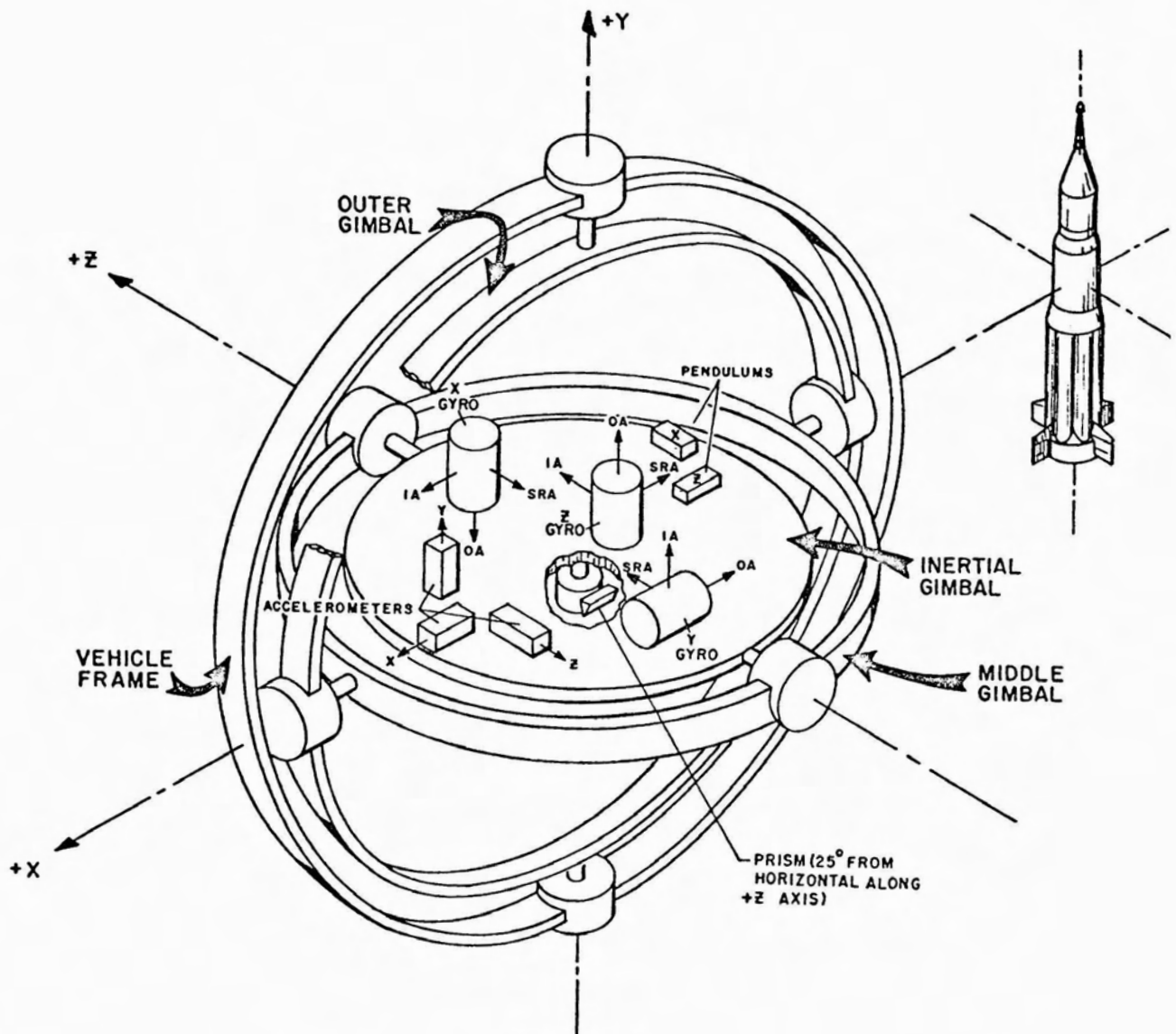


FIGURE 6
ST-124-M GIMBAL CONFIGURATION

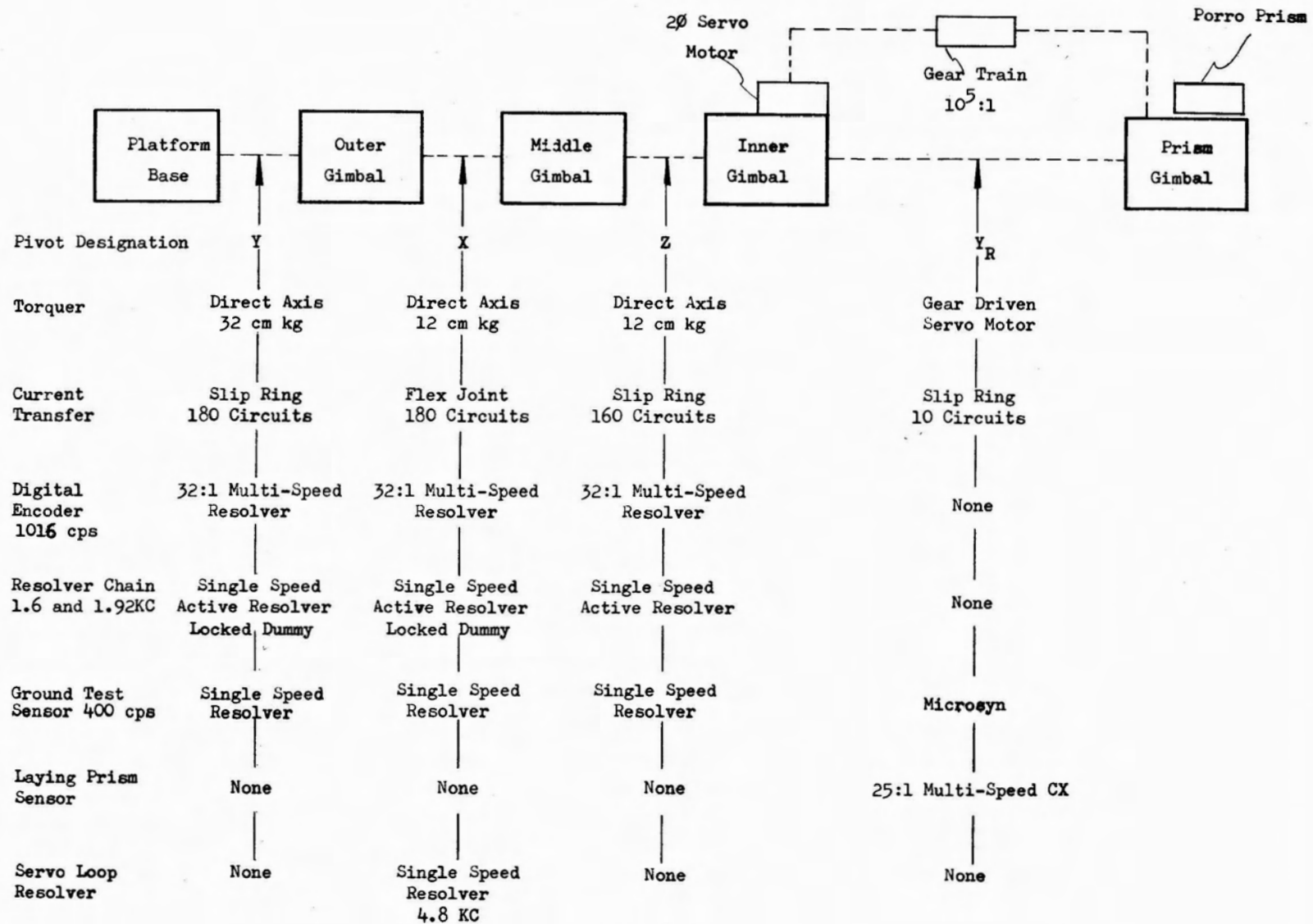


FIGURE 7
PLATFORM PIVOT CONFIGURATION

2.2 THE PLATFORM SERVO SYSTEM

Figure 8 is a block diagram of the platform gimbal servo loop. The servo loops are a 4.8 KC amplitude modulated carrier system with the gyro signal generator amplified and detected on the inner gimbal of the platform. A D.C. signal from the detector output is transferred through the platform slip rings and wiring to the Platform Servo Amplifier Assembly. The D.C. signal is modified by a lag second order lead stabilization network, remodulated at 4.8 KC, amplified and then re-detected prior to entering the D.C. power bridge. This D.C. power bridge provides a current source drive for the direct axis D.C. gimbal torquer. A 4.8 KC carrier was chosen to provide sufficient band width for the servo loop while a current driver for the torquer maintains the gain in the servo loop independent of torquer heating and commutator brush resistance.

The Z servo loop has the Z gyro signal generator amplified and sent to the Z pivot torquer (the inner most pivot of the platform) shown in Figure 8. The output of the X and Y gyro signal generators are resolved along the X, Y coordinates of the middle gimbal by a resolver mounted on the Z or inner pivot. These outputs of the resolver are amplified and detected on the middle gimbal as shown in Figure 8. The signal to the X servo amplifier card is amplified and fed to the X or middle pivot torque generator while the Y servo amplifier card drives the Y or outer pivot torquer. No gain compensation such as secant θ_X is used in the Y servo loop for middle gimbal angles $-45^\circ \leq \theta_X \leq 45^\circ$. The use of gain compensation in the Y loop will be discussed in paragraph 6.0.

The three accelerometer servo loops are identical and similar to the Z servo loop of Figure 8 with the exception of the torque generator which is mounted on the input axis of the accelerometer as shown in Figure 3.

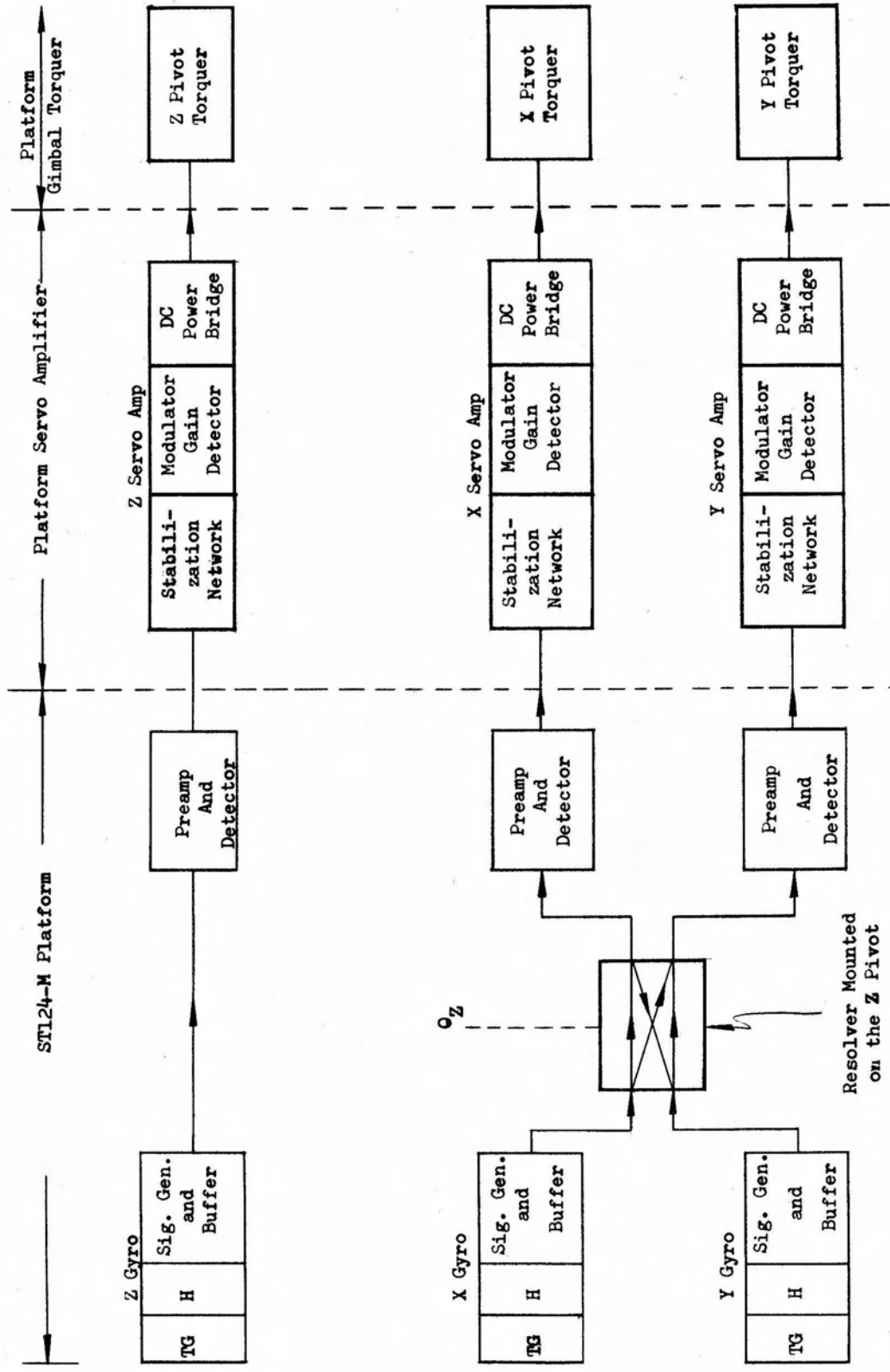


FIGURE 8
BLOCK DIAGRAM OF PLATFORM
GIMBAL SERVO LOOP

The servo loop signals to and from the platform are D.C. signals and at a high enough level so slip ring noise and resistance variations are negligible. The use of D.C. transmission was chosen to eliminate pickup and cable problems. Each servo loop has its own floating ground system with all loops referenced to the missile frame at one point to prevent ground loop coupling, and all amplifier stage design is push pull to eliminate coupling through the D.C. supply.

2.3 THE GIMBAL SENSORS

The X-Y-Z gimbal pivots have a single multi-speed resolver as shown in Figure 7. These resolvers are used as digital shaft encoders and a schematic block diagram is shown in Figure 9. The multi-speed resolver is the primary gimbal angle sensor for the attitude control system. The digital computer will process the measured gimbal attitude signals and compute the pitch, roll and yaw missile body rates for the attitude control system.

The resolver has both a multi-speed and single speed winding on the same magnetic structure. The multi-speed unit has 32 electrical rotations for one mechanical shaft rotation and its outer assembly winding is loaded with two R-C networks as shown in Figure 9.

The voltage V_2 at the input of the start pulse generator can be expressed as

$$\text{Eq. 1} \quad V_2 = \frac{E}{\sqrt{2}} e^{j [32 \theta - \pi/4]}$$

while the voltage V_3 at the input of the stop pulse generator can be expressed as

$$\text{Eq. 2} \quad V_3 = \frac{E}{\sqrt{2}} e^{-j [32 \theta - \pi/4]}$$

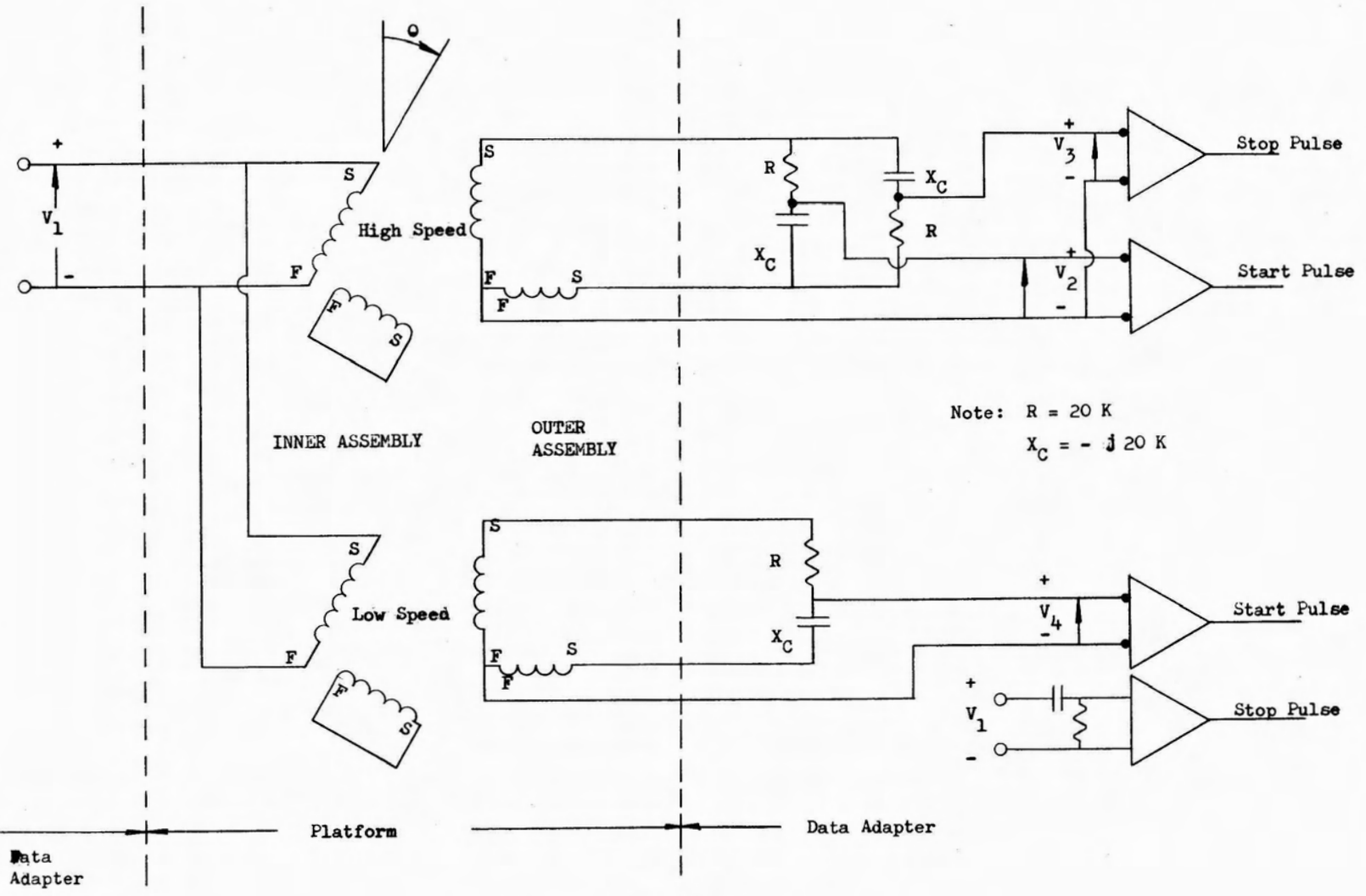


FIGURE 9
 SCHEMATIC BLOCK DIAGRAM OF PIVOT
 MULTI-SPEED RESOLVER DIGITAL ENCODER

where

E = The open circuit voltage of the resolver

θ = The gimbal angle in radians.

It can be seen from equations 1 and 2 that the phase shift of V_2 with respect to V_4 is 64 times the pivot angle, thus the double R-C network multiplies the machine speed by a factor of two.

As the instantaneous voltage V_2 passes through zero with a positive slope, a start pulse is generated which opens a gate and a counter counts a 2.048 MC clock frequency. As V_4 passes through zero with a positive slope, a stop pulse is generated which closes the gate and stops the counter. The number of cycles counted is a measure of shaft rotation.

The low speed winding is loaded with a single R.C. network which generates the start pulse. The stop pulse is obtained from the excitation voltage to the resolver inner assembly winding as shown in Figure 9. The method of counting is the same for the low speed winding.

The high speed system accuracy is basically insensitive to temperature variation of the resolver as well as impedance unbalances in the outer assembly winding since the open circuit voltage of the resolver is the basic reference voltage as shown in equations 1 and 2.

The performance characteristics of the encoder are

<u>Resolver Characteristics</u>	<u>32 Speed</u>	<u>Single Speed</u>
a. Excitation Voltage V_1	26 volt	Same
b. Excitation Frequency	1,016 cps	Same
c. Excitation Power	1.8 watts	0.08 watts
d. Secondary Voltage Max. (Open Circuit)	5.0 volts	5.0 volts
e. Mechanical Accuracy	± 10 arc sec.	± 30 arc min.

System Characteristics

a. System high speed	64:1
b. System low speed	1:1
c. Static Accuracy	± 30 arc sec.
d. Dynamic Accuracy (error is proportional to input rate)	20 arc sec. at 0.2 rad/sec.
e. Computer Clock Frequency	2.048 MC
f. Temperature Range for Optimum Accuracy	$\pm 30^\circ\text{C}$.

The ST124-M system also contains an analogue resolver chain system which can provide pitch, roll and yaw steering error signals directly to the control system. This is a backup scheme and presently it is not planned to fly.

The resolver chain system requires an inertial data box assembly which was not previously described. If not required to fly, this assembly will be used as a part of the ground checkout equipment.

The inertial reference box will contain three servoed driven resolvers whose shafts would be time programmed from the digital computer.

The resolver chain is shown in Figure 10 and the shafts $\alpha_Y, \alpha_X, \alpha_Z$ are time programmed from the digital computer. The resolver chain is excited with two frequencies, 26 volt 1.6 KC on the X_0 winding and 26 volt 1.92 KC on the Z_0 winding. These excitation frequencies are provided by the A.C. power supply.

A resolver has the characteristic of providing a linear transformation matrix from one vector space to another. Consider two orthogonal coordinate systems as shown in Figure 11. Let the $\bar{l}'_X, \bar{l}'_Y, \bar{l}'_Z$ coordinate system be rotated an angle α_X about the vector \bar{l}'_X to form the coordinate system $\bar{l}''_X, \bar{l}''_Y, \bar{l}''_Z$.

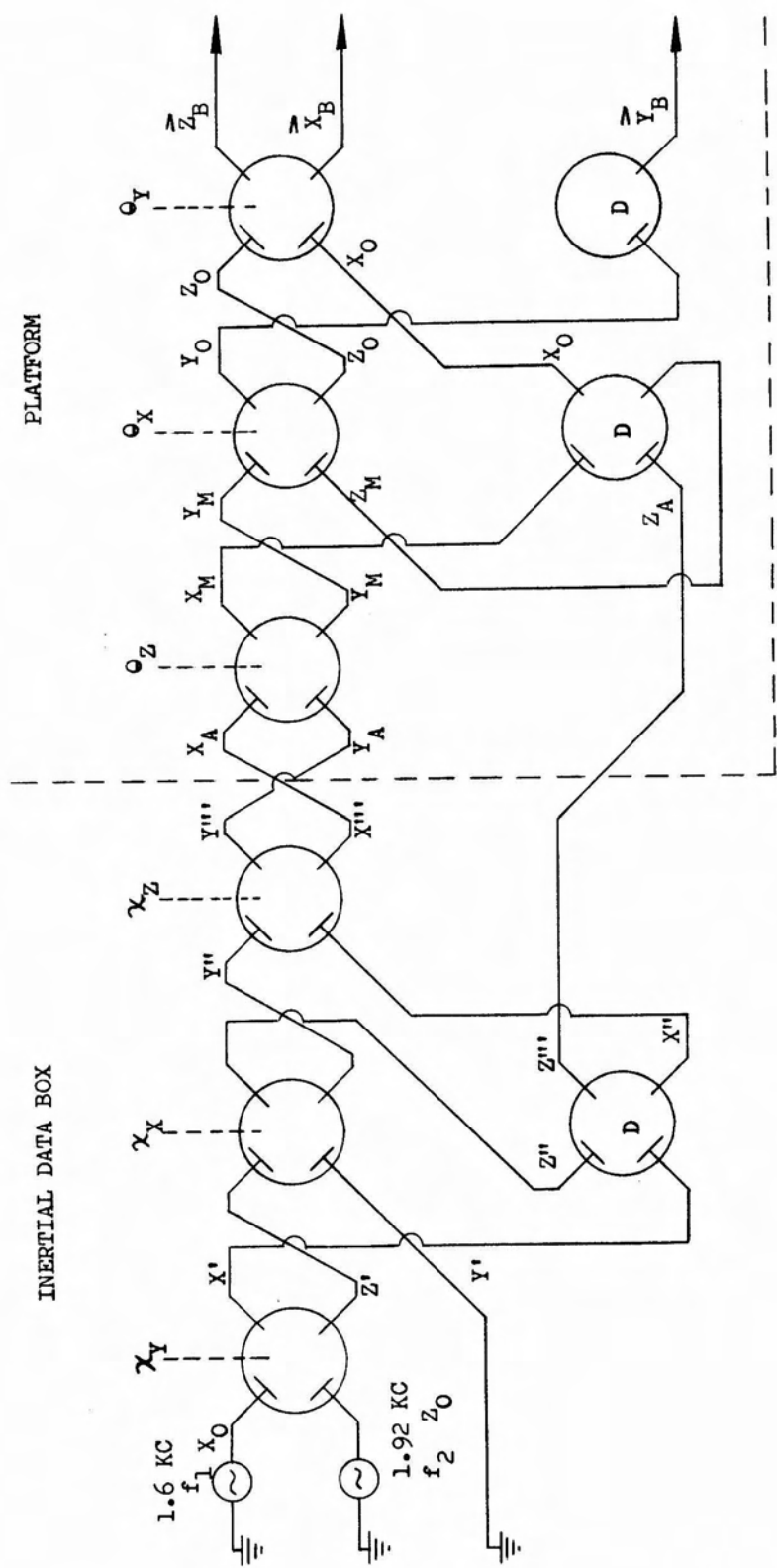


FIGURE 10
RESOLVER CHAIN ST124-M MOD III

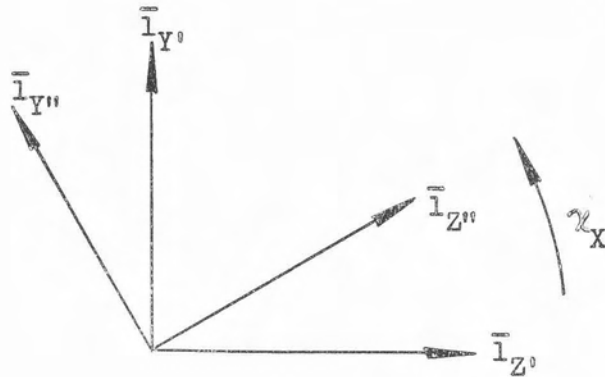


FIGURE 11
DEFINITION OF PRIME AND DOUBLE PRIME SPACES

The linear transformation relating a vector whose components are X' , Y' and Z' in the prime space to its components X'' , Y'' and Z'' in the double prime space can be expressed as

$$\text{Eq. 3} \quad \begin{bmatrix} X'' \\ Y'' \\ Z'' \end{bmatrix} = \begin{bmatrix} 1 & 0 & 0 \\ 0 & \cos \alpha_X & -\sin \alpha_X \\ 0 & \sin \alpha_X & \cos \alpha_X \end{bmatrix} \times \begin{bmatrix} X' \\ Y' \\ Z' \end{bmatrix}$$

The equation relating the output to the input of the α_X resolver in the inertial data box of Figure 10 is shown in equation 4.

$$\begin{aligned} \text{Eq. 4} \quad e_{Y''} &= (\cos \alpha_X) e_{Y'} - (\sin \alpha_X) e_{Z'} \\ e_{Z''} &= (\sin \alpha_X) e_{Y'} + (\cos \alpha_X) e_{Z'} \end{aligned}$$

Thus it can be seen that equations 3 and 4 are equivalent and if a locked resolver at zero angle is used for scaling the e_X component then the combination of an active resolver and a dummy winding will mechanize a linear transformation matrix.

From Figure 10 it can be seen that the resolver chain provides six transformation matrices.

Assume that the ideal missile body coordinates in space are \bar{l}_{XO} , \bar{l}_{YO} , \bar{l}_{ZO} and the orientation of this coordinate system is known with respect to the launch coordinates or the inner gimbal coordinate system. Then by first rotating the "O" coordinates α_Y about the Y vector, then α_X about the X vector and finally α_Z about the Z vector the "O" coordinate system will be coincident with the inner gimbal coordinate system. Let the actual missile body axis coordinate system be \bar{l}_{XB} , \bar{l}_{YB} , \bar{l}_{ZB} and assume that the 26 volt 1.60 KC excitation to the resolver chain is a unit vector along the \bar{l}_{XO} vector of the ideal missile yaw axis.

The resolver chain will transform the \bar{l}_{XO} unit vector into actual body axis "B" space as given by equation 5.

$$\text{Eq. 5} \quad \bar{l}_{XO} = a_{XB} \bar{l}_{XB} + a_{YB} \bar{l}_{YB} + a_{ZB} \bar{l}_{ZB}$$

Let the missile angular velocity perpendicular to the \bar{l}_{XB} vector (the yaw axis) be proportional to the vector cross product $[\bar{l}_{XO} \times \bar{l}_{XB}]$ then

$$\text{Eq. 5A} \quad \bar{w}_{\text{Missile}} \perp \text{to } \bar{l}_{XB} = a_{ZB} \bar{l}_{YB} - a_{YB} \bar{l}_{ZB}$$

Thus if the missile had a roll rate proportional to a_Z and a pitch rate proportional to $-a_{YB}$ the missile yaw axis $\bar{1}_{XB}$ would in the steady state be coincident with the ideal yaw axis $\bar{1}_{XO}$.

The 1.6 KC signal on the Z_B winding and the 1.6 KC signal on the Y_B winding at the output of the resolver chain would provide the required roll and pitch rates respectively.

Assume that the 26 volt 1.92 KC excitation to the resolver chain is a unit vector along the $\bar{1}_{ZO}$ vector of the ideal missile pitch axis. The resolver chain will transform the $\bar{1}_{ZO}$ unit vector into actual body axis "B" space as given by equation 6.

$$\text{Eq. 6} \quad \bar{1}_{ZO} = b_{XB} \bar{1}_{XB} + b_{YB} \bar{1}_{YB} + b_{ZB} \bar{1}_{ZB}$$

Let the missile yaw velocity be proportional to the $\bar{1}_{XB}$ component of the vector cross product $[\bar{1}_{ZO} \times \bar{1}_{ZB}]$ then

$$\text{Eq. 7} \quad \bar{1}_{ZO} \times \bar{1}_{ZB} = b_{YB} \bar{1}_{XB} - b_{XB} \bar{1}_{YB}$$

Thus if the missile yaw rate is proportional to b_{YB} the missile body axis coordinate system in the steady state would be coincident with the ideal coordinate system $\bar{1}_{XO}, \bar{1}_{YO}, \bar{1}_{ZO}$.

The roll, pitch and yaw rate signals are shown in Figure 12. When the missile coordinate system is aligned to the ideal coordinate system the Z_B winding of the resolver chain will have a standing voltage of 15 volts 1.92 KC which is the $\bar{1}_{ZO}$ vector transformed to the body axis space. This bias voltage is removed by a bucking voltage and the resulting voltage a_{ZB} is fed to a Command Voltage Demodulator module in the inertial data box. The signal is detected, amplified, redetected and the output is a D.C. signal with a scale factor of 3 volt/deg.

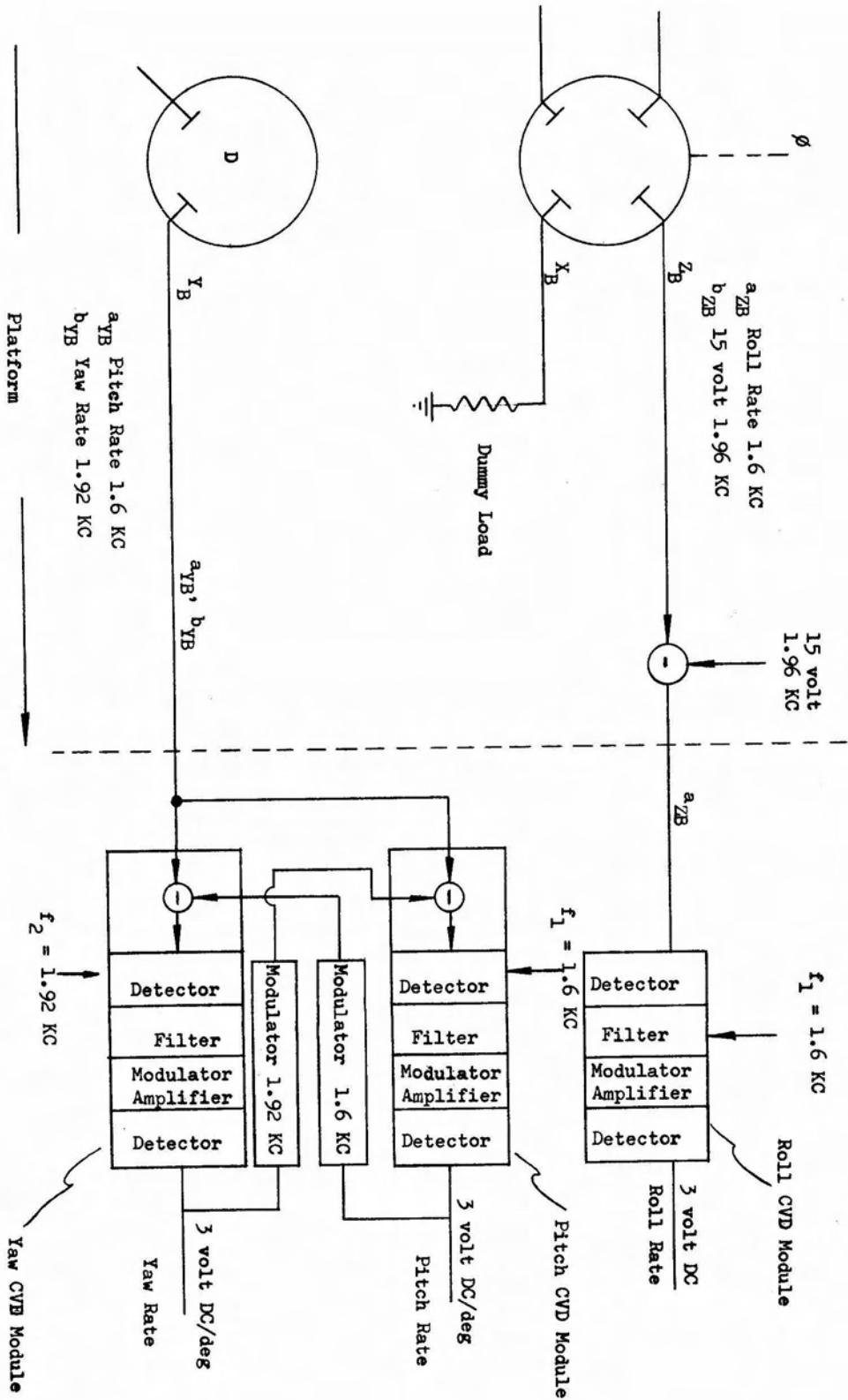


FIGURE 12
RESOLVER CHAIN OUTPUT BLOCK DIAGRAM

The signal on the X_B winding is a redundant roll signal plus a 15 volt 1.6 KC signal which is the \bar{l}_{XO} vector transformed to body axis space. This winding is not used and terminated with a dummy load.

The signals on the Y_B winding are a_{YB} pitch rate 1.6 KC and b_{YB} yaw rate 1.92 KC. There is no standing voltage on this winding. Both signals are fed to CVD modules in the inertial data box. By a means of signal bucking, detection filtering, modulation amplification and re-detection, the two signals a_{YB} and b_{YB} are separated as shown in Figure 12. The output signals for both yaw and pitch rate are D.C. with a scale factor of 3 volt/degree.

The 3 σ accuracy of the resolver chain is 6 arc minutes over the complete sphere. The use of the resolver chain for ground checkout will be described in paragraph 2.6.

2.4 THE ERECTION SYSTEM

The inner gimbal of the platform carries two gas bearing leveling pendulums, whose input axis are along the \bar{l}_{XA} and \bar{l}_{ZA} vectors of the inner gimbal as shown in Figure 6.

The gas bearing pendulum is a single axis device whose sensing element is a gas floated slug which supports a soft iron core as shown in Figure 13. The iron slug moves inside the coils of a linear differential transformer which provides the electrical output signal. Damping of the slug motion is provided by a chamber and an exhaust orifice while the spring restraint is obtained electromagnetically from a taper on the soft iron core.

64-3229

DIFFERENTIAL
TRANSFORMER
COILS

GAS INLET

FLOATING SLUG

IRON SLEEVE
(DIFFERENTIAL
TRANSFORMER
CORE)

DAMPING
CHAMBER

GAS EXHAUST

GAS BEARING
SLEEVE

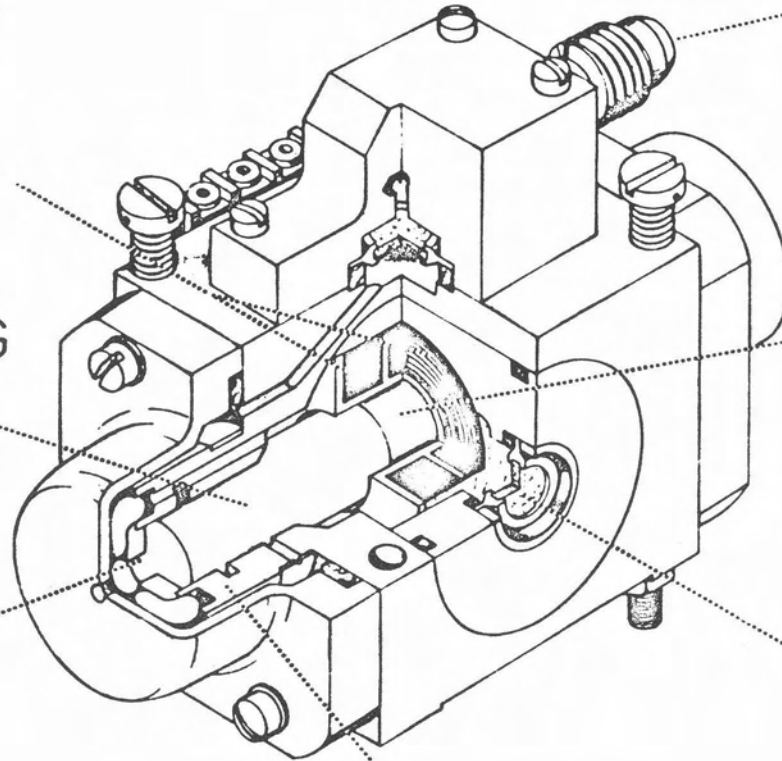


FIGURE 13

GAS BEARING PENDULUM

The characteristics of the pendulum are

a. Excitation Voltage	4.0 volt 400 cps
b. Scale Factor	0.3 volt/degree
c. Null Repeatibility	± 5 arc sec
d. Base Alignment	± 5 arc sec
e. Max. Tilt Angle	± 0.5 degree
f. Linearity	$\pm 2\%$

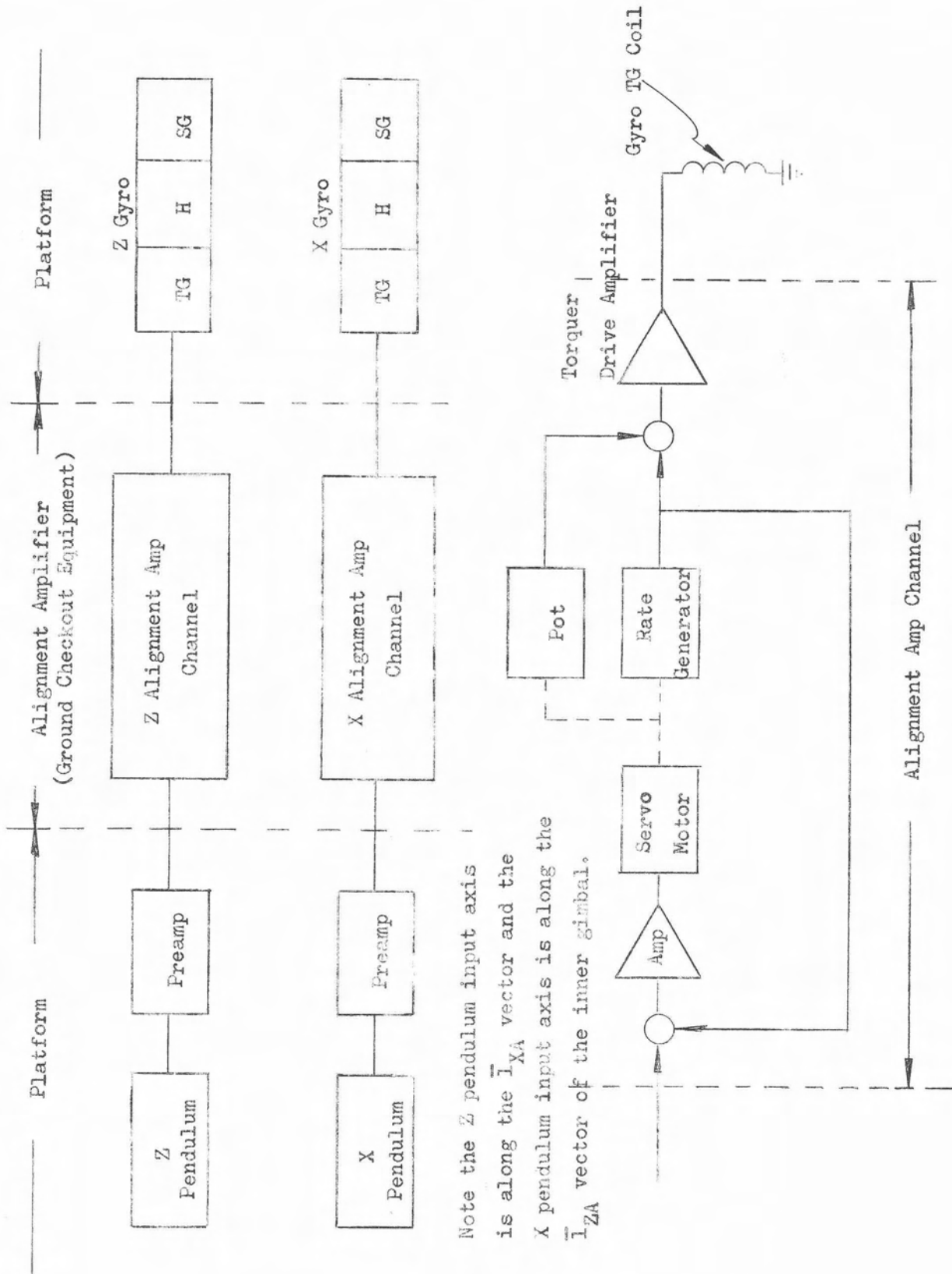
The block diagram of the erection system is shown in Figure 14. The X and Z pendulum have their input axis along vectors \bar{l}_{ZA} and \bar{l}_{XA} of the inner gimbal respectively. The pendulum output is amplified by a pre-amplifier in the platform and then transmitted to the ground equipment alignment amplifier.

The alignment amplifier provides a proportional plus integral path to the torque drive amplifier, which returns the signal from the ground to the platform gyro torque generator variable coil.

The erection system is basically a second order system with a natural frequency of 0.05 radian/sec and a damping ratio of 0.5 with a leveling accuracy of ± 5 arc seconds.

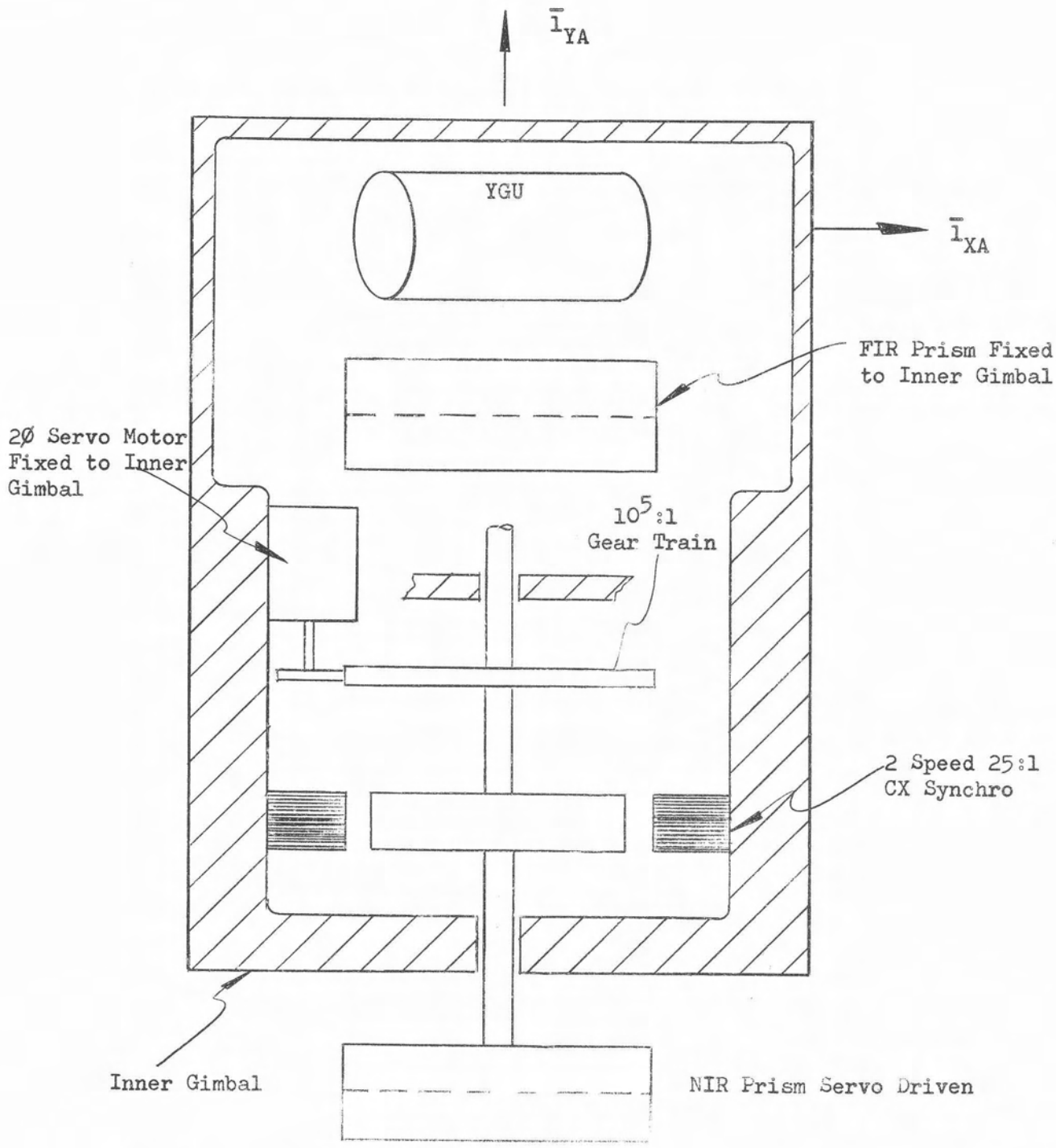
2.5 THE AZIMUTH LAYING SYSTEM

The inner gimbal contains a fixed prism (FIR) and a servoed driven prism (NIR) as shown in Figure 15. The fixed prism has its porro edge parallel to the \bar{l}_{XA} vector while the porro edge of the movable prism will rotate in the $\bar{l}_{XA}, \bar{l}_{ZA}$ plane. The movable prism is driven by a 2ϕ servo motor mounted to the inner gimbal through a gear train of $10^5:1$ and the angle between the prism and the inner gimbal is measured by a $25:1$ two speed control transmitter synchro.



Note the Z pendulum input axis is along the \bar{I}_{XA} vector and the X pendulum input axis is along the \bar{I}_{ZA} vector of the inner gimbal.

FIGURE 14
ERECTION SYSTEM BLOCK DIAGRAM



NOTE: \bar{i}_{ZA} points out of paper.

FIGURE 15
INNER GIMBAL LAYING SYSTEM SCHEMATIC

The azimuth alignment block diagram is shown in Figure 16. Assume that the inner gimbal is erected to the launch vertical, then a base line azimuth is obtained by closing the encoder repeater servo through contact D and the Y gyro alignment loop through contact A.

The inner gimbal prism (FIR) error signal is transmitted from the theodolite through contact A to the Y gyro alignment loop which will position the inner gimbal to the base line azimuth. At the same time, the servoed prism (NIR) error signal from the theodolite will drive the 2ϕ servo motor on the inner gimbal so the movable prism is aligned along the same base line. The encoder servo will follow the two speed synchro on the inner gimbal and the 18 bit encoder signal will be stored in the ground based digital computer. This stored signal is a calibration of the zero alignment transmission errors in the synchro system.

The mission azimuth is established by opening contacts A, D and closing contacts B and C. The ground based digital computer computes a mission azimuth and programs the 18 bit encoder to its desired shaft position. The error signal from the two speed synchro system is fed to the Y alignment loop and drives the inner gimbal to its mission azimuth as the servoed prism (NIR) is held fixed with respect to the optical beam from the theodolite or base line azimuth.

The laying system has an accuracy of ± 20 arc seconds.

2.6 THE ST124-M SYSTEM BLOCK DIAGRAM

The ST124-M system configuration has been described, and its operation in different modes detailed by individual block diagrams and schematics. Figure 17 is a guidance system interconnection drawing showing a complete system block diagram. The platform provides thrust velocity signals to the accelerometer signal conditioner which are then sent to the data adapter and airborne digital computer.

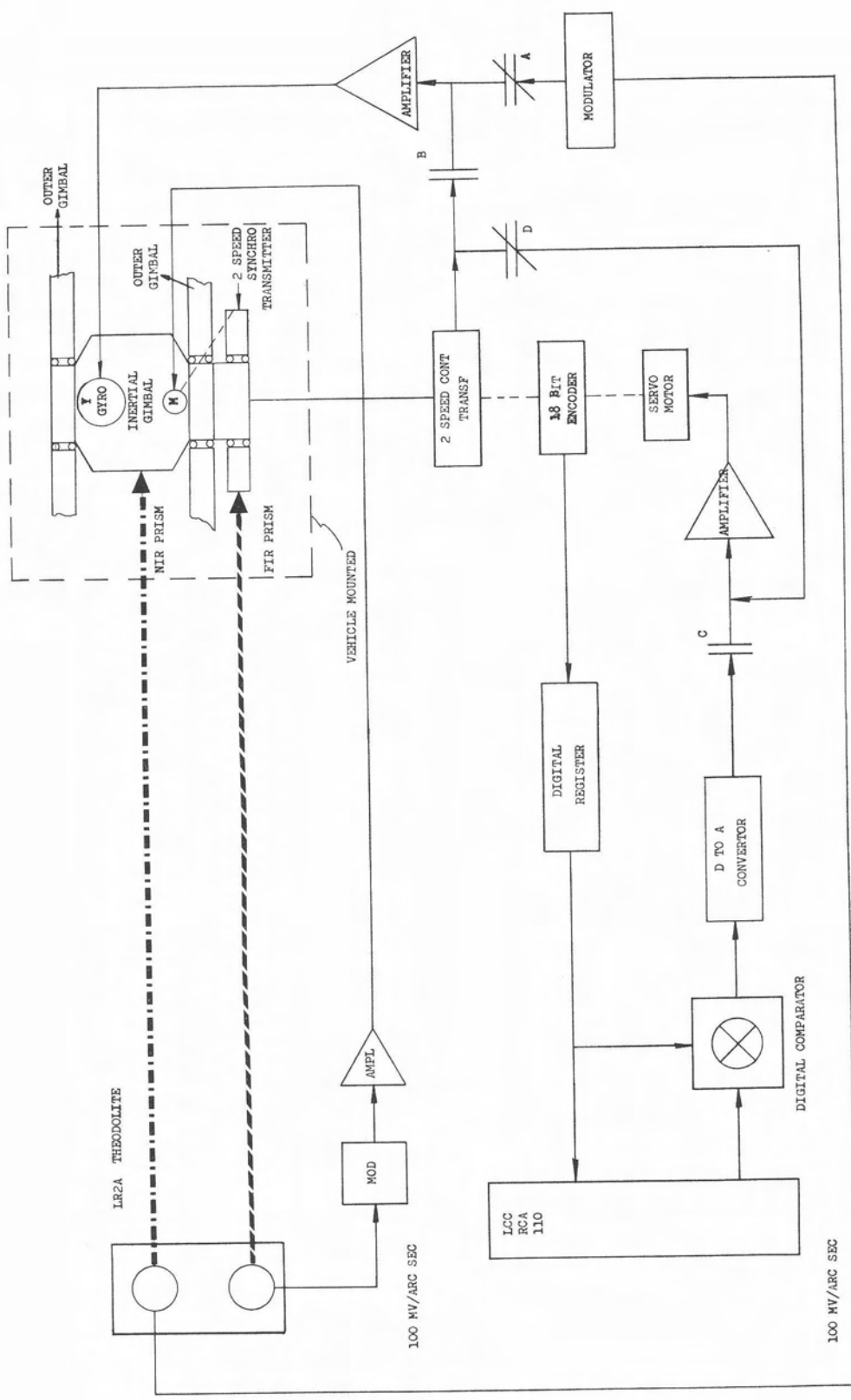


FIGURE 16
AZIMUTH ALIGNMENT BLOCK DIAGRAM

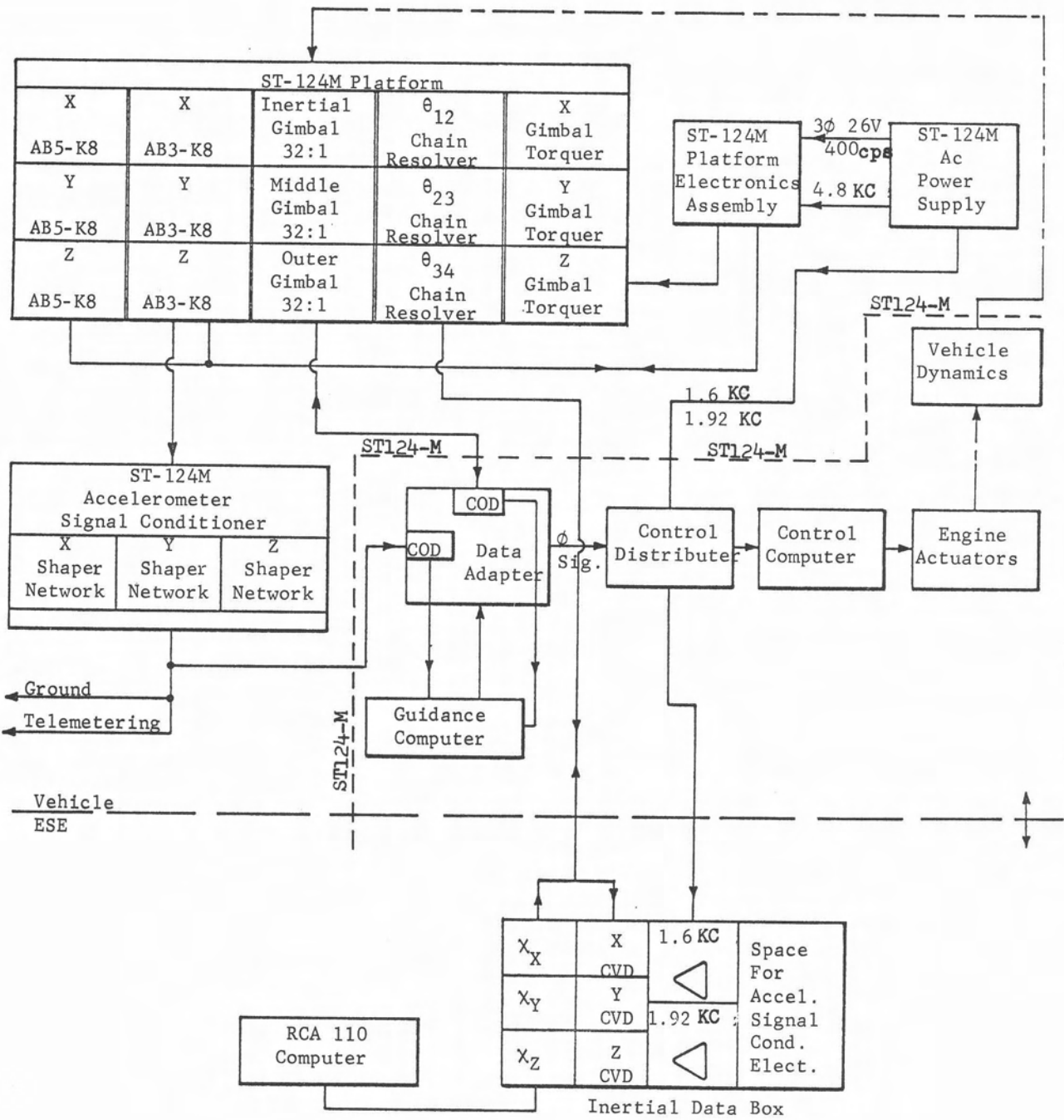


FIGURE 17
GUIDANCE SYSTEM INTERCONNECTION
BLOCK DIAGRAM

The platform gimbal multi-speed resolvers are coupled to data adapter then to the computer. The platform servo amplifier assembly closes the six servo loops while the A.C. power supply supplies 400 cps and 4.8 KC power to the servo amplifier. The A.C. power supply also supplies the 1.6 KC, 1.92 KC excitation voltages to the inertial data box resolver chain. The inertial data box is part of the ground equipment and is used for ground test and checkout. The ground based digital computer programs the γ_X , γ_Y and γ_Z shafts and the error signals from the output of the resolver chain are fed to the alignment amplifier to position the platform gimbals in different attitudes during the prelaunch test mode.

SECTION 3.0

THE INERTIAL COMPONENTS

The ST124-M stable platform contains three AB5-K8 gas bearing single degree of freedom gyros and three AB3-K8 gas bearing pendulous gyro accelerometers. These components measure the vehicle motion and their performance capabilities define the hardware accuracy of the guidance system. No compensation is used in the digital computer for instrument error terms and absolute tolerances are established for the life of the instruments.

3.1 THE AB5-K8 STABILIZING GYRO

The AB5-K8 gas bearing gyro is a single degree of freedom component and is shown in a cut away view in Figure 18. The gyro wheel (B) shown in Figure 19 mounts in a yoke of the cylinder end cap (A), and the necked section of the yoke is controlled to minimize the anisoelastic drift of the cylinder assembly. The cylinder end cap (A) mounts in the cylinder C forming the gyro cylinder assembly. The cylinder assembly with the exception of the gyro wheel is beryllium and is filled with a helium atmosphere.

The cylinder (A) is suspended in a hydrostatic gas bearing between the sleeve (B) and endplates (C) (D) shown in Figure 20, providing both radial and axial centering. The endplates are bolted to the sleeve and this assembly forms the case of the gyro.

Dry gaseous nitrogen is passed through two rows of 24 holes with millipore discs in the sleeve acting as flow restrictors. The gas in the cylinder chamber generates the hydrostatic bearing, and then it escapes around the hub at each end of the cylinder. The sleeve and endplates are beryllium with machined tolerances of 20 microinches in roundness and 20 microinches per inch in squareness. The cylinder also has the same type of tolerances.

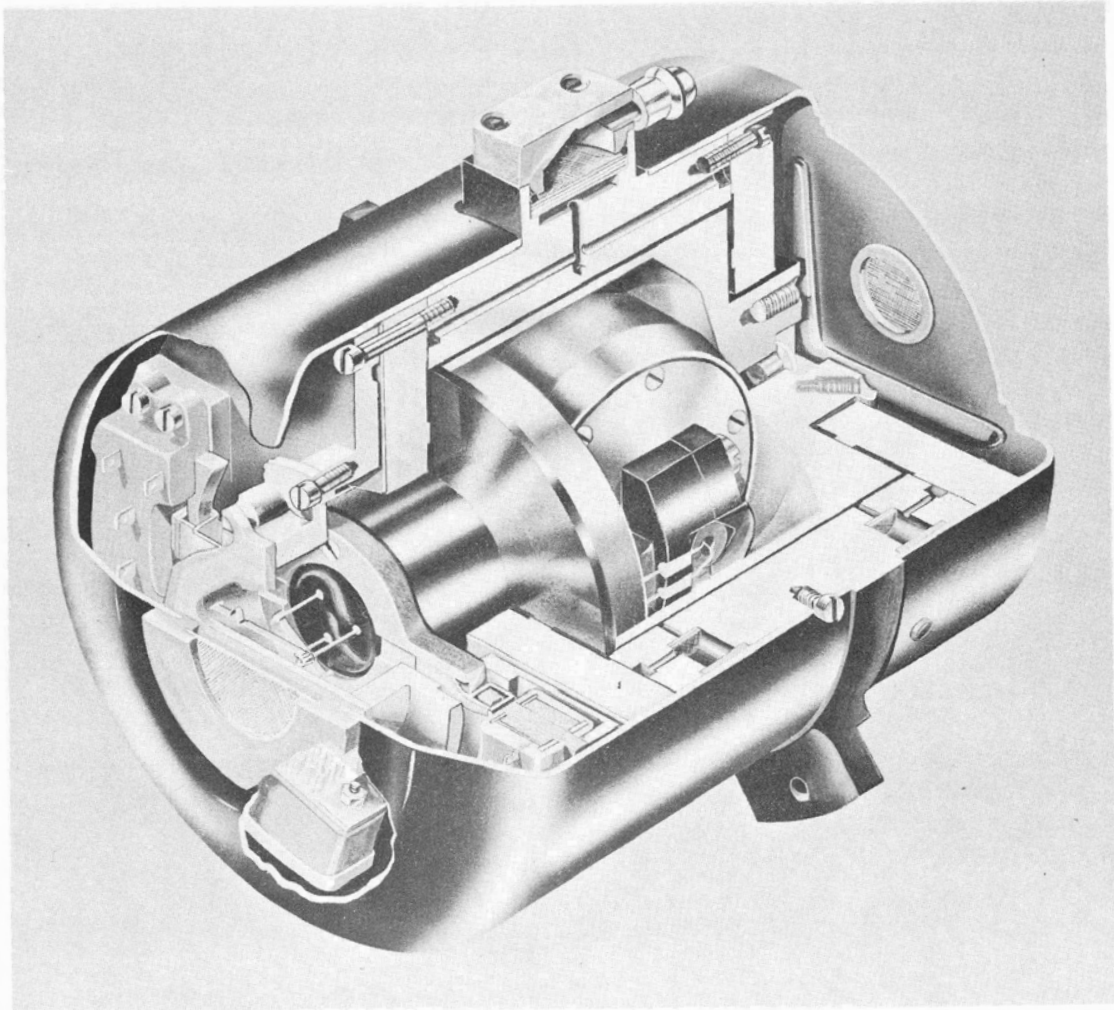


FIGURE 18
SATURN AB5-K8 GYRO ASSEMBLY

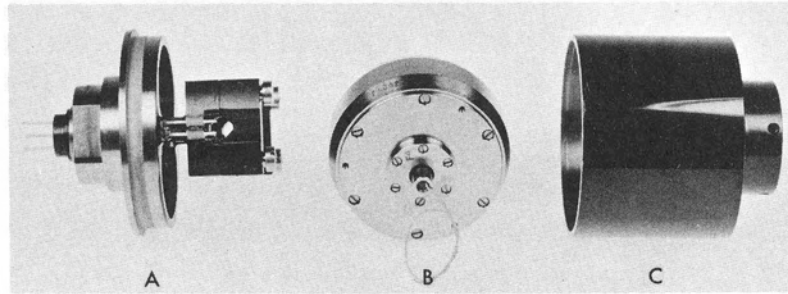


FIGURE 19
SATURN AB5-K8 INNER CYLINDER ASSEMBLY

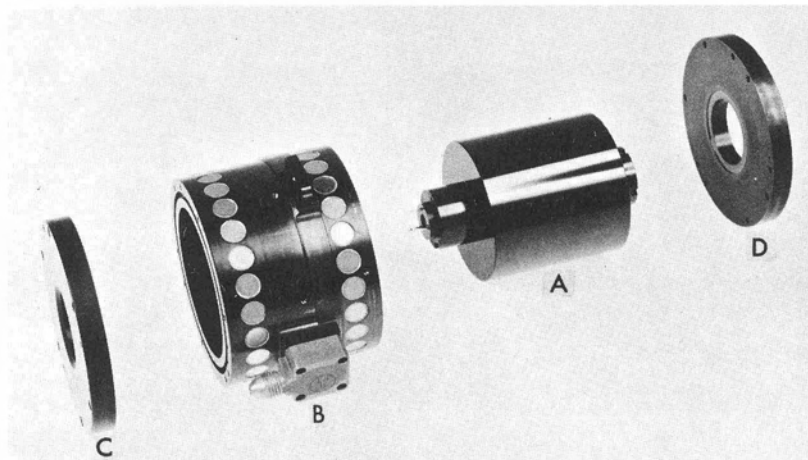


FIGURE 20
SATURN AB5-K8 GAS BEARING ASSEMBLY

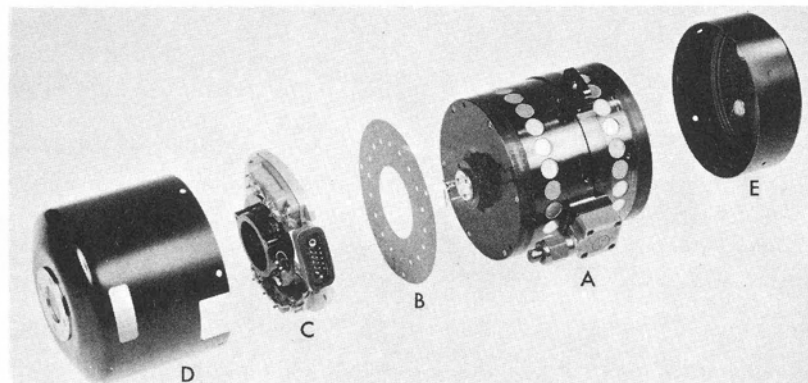


FIGURE 21
AB5-K8 GYRO ASSEMBLY

The signal generator and torque generator are shown in (C) of Figure 21. They are coupled to the cylinder by means of a copper shorted turn which is mounted on the cylinder. The standoff's for the flex leads can be seen on the float of (A). These flex leads are terminated on studs mounted in assembly (C) of Figure 21. A magnetic shield (B) is placed between the gyro case (A) and the signal generator (C). Dust covers (D) and (E) complete the assembly.

The gyro characteristics are listed below

1. Gyro Wheel

a. Type	Synchronous hysteresis
b. Angular momentum	$2 \times 10^6 \text{ g cm}^2/\text{s}$
c. Wheel speed	24,000 rpm
d. Wheel excitation	26 volt, 3 phase, 400 cps
e. Wheel bearing preload	3.4 kg operating
f. Wheel power at sync	10 watts
g. Wheel life	3000 hours minimum
h. Wheel mount	Symmetrical
j. Wheel sync time	90 seconds

2. Gas Bearing

a. Gas pressure	15 psig
b. Gas flow rate	2000 cc/min STP
c. Gas gap	0.0015 cm to 0.002 cm
d. Orifice restrictors	Millipore discs
e. Sleeve material	Anodized beryllium
f. End plate material	Anodized beryllium
g. Cylinder material	Anodized beryllium

3. Signal Generator

a. Type	Shorted turn reluctance
b. Excitation	10 volts, 4.8 KC
c. Sensitivity	550 millivolts/degree with 10 k Ω load
d. Float freedom	± 3 degrees $\begin{matrix} + 0^\circ \\ - 0.5^\circ \end{matrix}$

4. Torque Generator (for prelaunch erection only)

- | | |
|-------------------------------------|-------------------------|
| a. Type | Shorted turn reluctance |
| b. Normal erection rate | 6 degrees/min |
| c. Fixed coil excitation | 26 volt, 400 cps, 45 mA |
| d. Maximum variable coil excitation | 30 volt, 400 cps, 50 mA |

5. Physical Characteristics

- | | |
|-------------|-----------------------------|
| a. Size | 3" dia. by 4" length |
| b. Weight | 900 grams |
| c. Mounting | Three-point flange mounting |

3.2 THE AB3-K8 PENDULOUS GYRO ACCELEROMETER

The AB3-K8 instrument is a pendulous gyro accelerometer and is shown schematically in Figure 22.

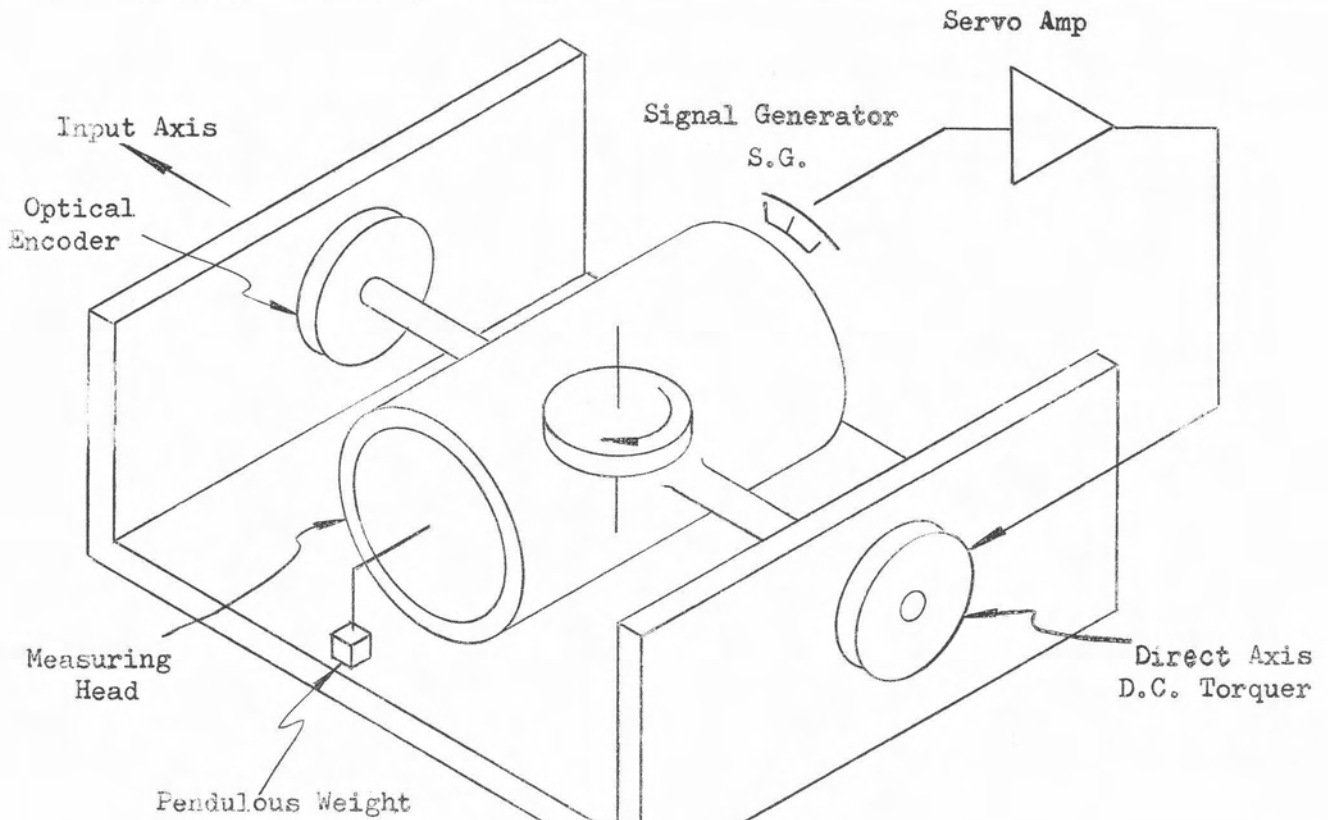


FIGURE 22
AB3-K8 SCHEMATIC

The accelerometer is a single degree of freedom gyro with a pendulous cylinder mounted in a pair of pivots and free to rotate with respect to its housing. A servo loop is closed from the gyro output axis signal generator to a direct axis torquer which is mounted on the input axis thus stabilizing the measuring head and holding the pendulous weight perpendicular to the input axis.

The speed of the measuring head with respect to inertial space is proportional to thrust acceleration along the input axis and the position of the measuring head is a measure of thrust velocity.

The accelerometer has a scale factor of 300 meter sec^{-1} /revolution, a pendulosity of 20 gram cm and an angular momentum of 10^5 gram $\text{cm}^2 \text{sec}^{-1}$.

An optical incremental encoder is mounted on the input axis and provides a measure of thrust velocity. It has a minimum bit count of 0.05 meter sec^{-1} /bit.

The single degree of freedom gyro is constructed the same as the AB5-K8 gyro with the exception that the endplates are fabricated of monel so as to lower the servo loop nutation frequency. A cut away of the accelerometer is shown in Figure 23.

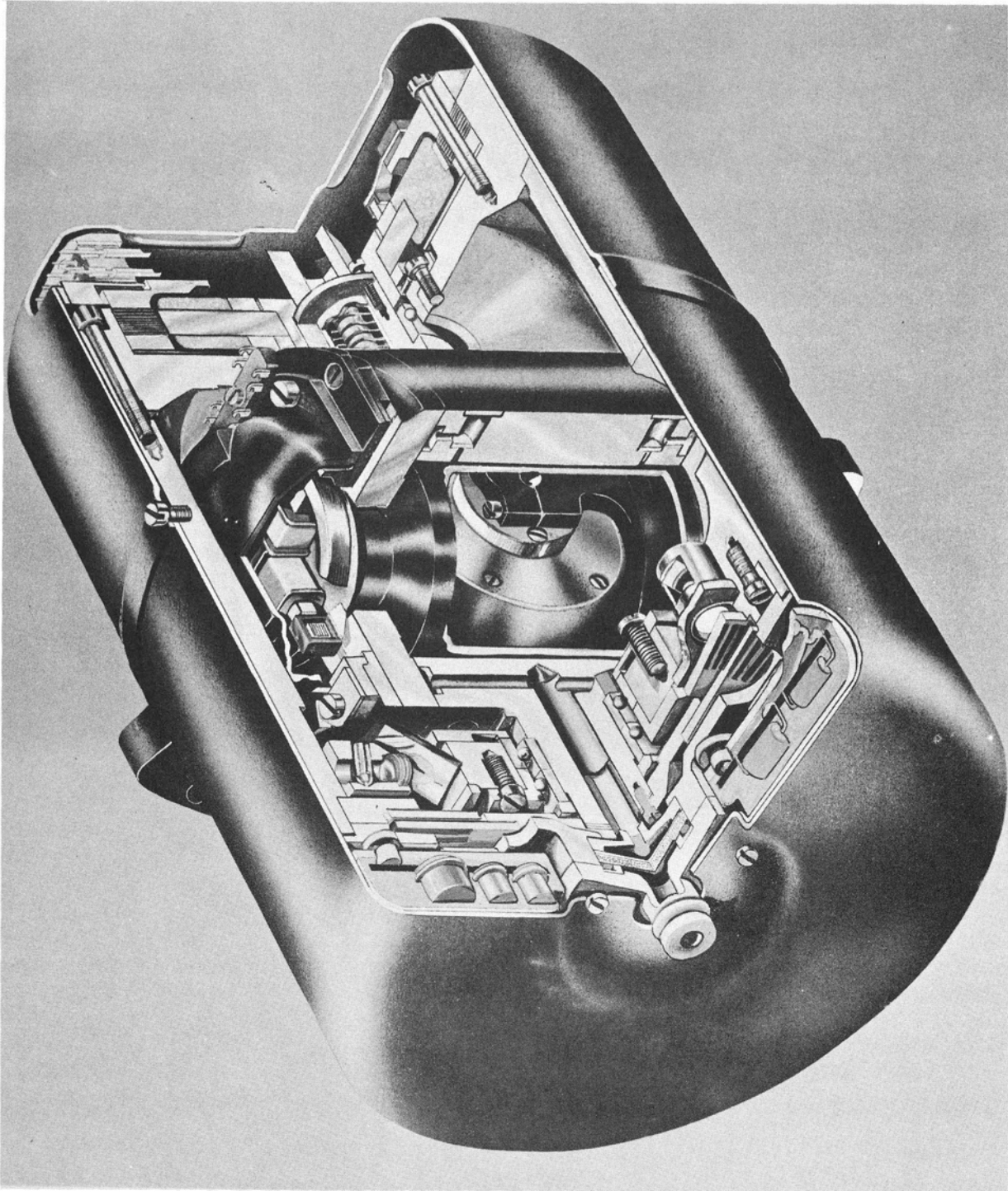


FIGURE 23
AB3-K8 INTEGRATING GYRO ASSEMBLY

The accelerometer characteristics are listed below.

1. Gyro Wheel

a. Type	Synchronous hysteresis
b. Angular momentum	1×10^5 g cm ² /s
c. Wheel Speed	12,000 rpm
d. Wheel excitation	26 volts, 3 phase, 400 cps
e. Wheel sync time	90 seconds
f. Wheel power at sync	4.5 watts
g. Wheel life	3000 hours minimum
h. Wheel mount	symmetrical
j. Wheel bearing preload	907.2 g operating

2. Gas Bearing

a. Gas pressure	15 psig
b. Gas flow rate	2400 cc/min STP
c. Gas gap	0.0015 cm to 0.002 cm
d. Orifice restrictors	Millipore discs
e. Sleeve material	Anodized beryllium
f. Endplate material	Monel with optical encoder pick-off
g. Cylinder material	Anodized beryllium

3. Signal Generator

a. Type	Four-pole shorted turn reluctance
b. Excitation	10 volts, 4.8 KC
c. Sensitivity	285 millivolts/degree with 10 k Ω load
d. Float freedom	± 3 degrees $\begin{matrix} +0^\circ \\ -0.5^\circ \end{matrix}$

- 4. Torque Motor
 - a. Type Direct axis DC torquer
 - b. Maximum torque 1.440 kg cm at 1.1A ; 44 volts

- 5. Velocity Pick-Off
 - a. Type Digital encoder (optical grid)
 - b. Count 6000 counts per revolution
 - c. Resolution 0.05 m/s/bit
 - d. Output Incremental with redundant channels

- 6. Physical Characteristics
 - a. Size 3.25" dia. by 5" length
 - b. Weight 1200 grams
 - c. Mounting Three-point flange mounting

- 7. Performance
 - a. Accelerometer scale factor 300 meters per second per revolution of output axis

$W_{ICZC} \triangleq$ the angular rate of the stabilized gimbal with respect to inertial space, the input axis "Z" component in gimbal or case space.

Consider the loop broken at point "B" then the open loop gain is

$$\text{Eq. 8} \quad A(p) = \frac{H^2}{J_g J_G p^2} \left[1 + \frac{G(p)}{H_p} \right]$$

Define the nutation frequency of the loop as

$$\text{Eq. 9} \quad W_g = \frac{H}{[J_g J_G]^{1/2}}$$

then non dimensionalizing equation 8 with respect to W_g

$$\text{Eq. 10} \quad A(u) = \frac{1}{u^2} \left[1 + \frac{G(u)}{H W_g u} \right]$$

The function $A(u)$ has 270° of lag if $G(u)$ were a constant, thus if $G(u)$ is to stabilize the loop it will have to provide better than 90° of lead. This requires a quadratic lead function. Assume an amplifier function as given in equation 11

$$\text{Eq. 11} \quad G(u) = K_1 \left\{ \frac{u^2}{v_n^2} + 2\zeta_n \frac{u}{v_n} + 1 \right\}$$

Substituting equation 11 in 10 the open loop gain becomes

$$\text{Eq. 12} \quad A(u) = \frac{K}{u^3} \left\{ \frac{u^2}{v_n^2} + 2 \left(\zeta_n + \frac{v_n}{2K} \right) \frac{u}{v_n} + 1 \right\}$$

where

$$\text{Eq. 13} \quad K = \frac{K_1}{H W_g}$$

It can be seen that equation 12 can be stabilized by the proper choice of K , ζ_n and v_n . A possible choice of values is

$$\begin{aligned} v_n &= 1.5 \\ \zeta_n &= 0.5 \\ K &= 5.0 \end{aligned}$$

A lag network will be added to the amplifier transfer function in equation 11 to increase the D.C. stiffness at zero frequency and will be removed at a low enough frequency so as not to effect the stability of the loop.

Since it is physically impossible to generate a quadratic function as shown in equation 11 a quadratic lag must be added to the denominator of this equation. A realizable lag network and band pass for the lag lead network is shown in equation 14

$$\text{Eq. 14} \quad \frac{G(u)}{H_w g} = 22 \frac{\left[\frac{u}{0.3} + 1 \right]}{\left[\frac{u}{0.07} + 1 \right]} \times \frac{\left[\frac{u^2}{(1.5)^2} + \frac{u}{1.5} + 1 \right]}{\left[\frac{u^2}{(15)^2} + \frac{u}{15} + 1 \right]}$$

When synthesizing an actual network the amplifier transfer function is

$$\text{Eq. 15} \quad \frac{G(u)}{H_w g} = 30 \frac{\left[\frac{u}{0.29} + 1 \right] \left[\frac{u}{18.8} + 1 \right] \left[\frac{u^2}{(1.16)^2} + \frac{2(0.68)u}{1.16} + 1 \right]}{\left[\frac{u}{0.073} + 1 \right] \left[\frac{u}{10.5} + 1 \right] \left[\frac{u^2}{(20.6)^2} + \frac{2(0.8)u}{20.6} + 1 \right]}$$

The fourth order equation is obtained from impedance loading in attempting to generate the ideal function of equation 14.

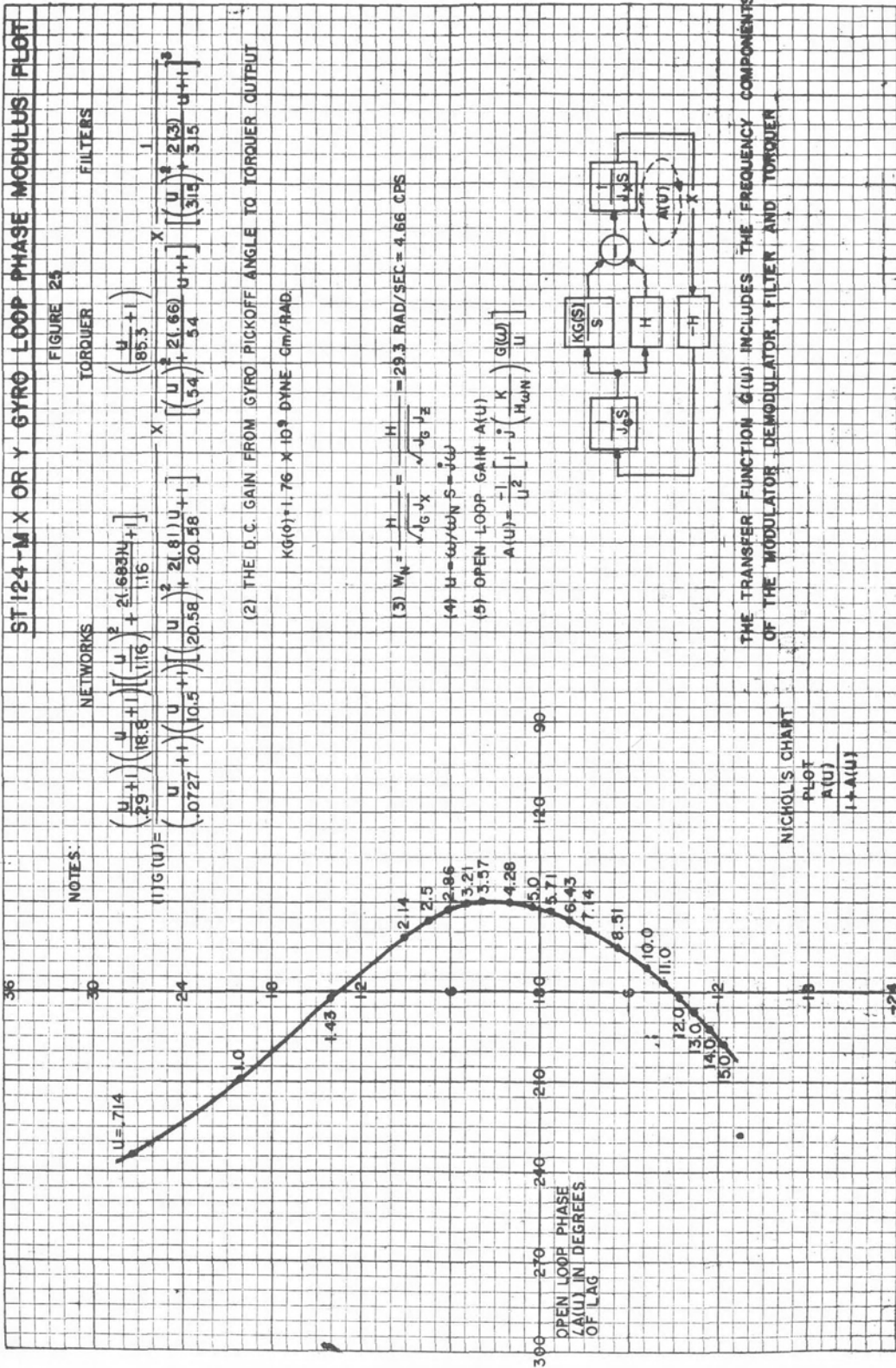
A phase modulus plot of the $A(u)$ function for the X or Y gyro loop is shown in Figure 25. The nutation frequency of the loop is 4.66 cps and it has a static stiffness of 1.76×10^9 dyne cm/radian of gyro pickoff displacement.

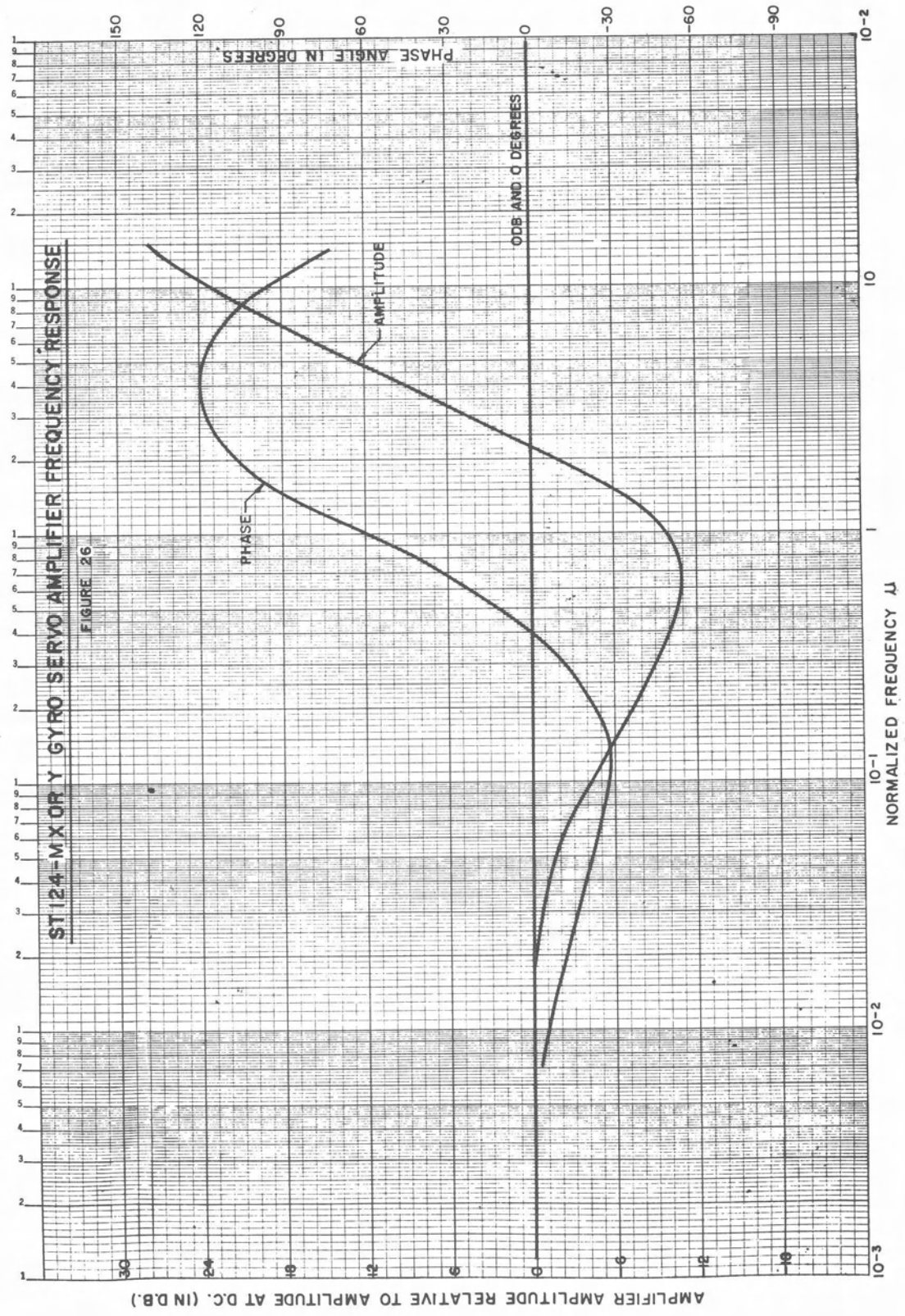
The phase modulus plot has a plus 13 db and minus 9 db gain margin and a 28° phase margin. The resonance rise in the loop is 6db.

Figure 26 is a frequency response plot of the servo amplifier. It can be seen that 90° lead occurs at $u=1.5$ and the lead network has a band width of 7.5, with a maximum lead angle of 120° at $u=4$. The effect of the lag network can be seen from $u=0.07$ to $u=0.3$. The amplifier gain has its minimum value in the vicinity of the nutation frequency, however, the amplifier is capable of delivering maximum torque at the notch point within the limit stops of the gyro. The frequency response plot and the ideal network agree with sufficient accuracy to provide a stable loop.

ST 124-M X OR Y GYRO LOOP PHASE MODULUS PLOT

FIGURE 25





SECTION 5.0

THE PLATFORM CHARACTERISTIC EQUATION

The single axis servo analysis will not adequately describe a three gimbal platform since with the gimbal angles at any arbitrary attitude, the X, Y and Z gimbal servo loops are possibly coupled together.

By describing the complete equations of motion for a platform and neglecting all non-linear terms, it is possible to derive the signal flow diagram shown in Figure 27. All solid lines in the signal flow graph describe the platform kinematic equations and are present without any electronics coupled to the platform. The dashed lines in the signal flow graph represent the platform electronic paths.

The following definitions will be helpful in reading the graph

$W_{IAXA}, W_{IAYA}, W_{IAZA} \stackrel{\Delta}{=} \text{Components of the angular velocity of the inner gimbal with respect to inertial space written in "A" space. These three variables are the dependent variables of the system.}$

$A_X, A_Y, A_Z \stackrel{\Delta}{=} \text{The float angular displacement of the X, Y, and Z gyro.}$

$M_{XTG}, M_{YTG}, M_{ZTG} \stackrel{\Delta}{=} \text{The gimbal torquer moments of the X, Y, and Z pivot torquers.}$

$G_X, G_Y, G_Z \stackrel{\Delta}{=} \text{The X, Y, and Z servo amplifier transfer function.}$

$M_{DX}, M_{DY}, M_{DZ} \stackrel{\Delta}{=} \text{Acceleration sensitive moments (due to pendulous gimbals) about the X, Y, Z pivots.}$

$M_{FX}, M_{FY}, M_{FZ} \stackrel{\Delta}{=} \text{The friction moments about the X, Y, and Z pivots.}$

$$J_{XXA} = J_{XX} - J_{XYA} \cos 2 \phi_Z$$

$$J_{XX} = J_{AXX} + J_{MXX} + J_{XYA}$$

$$J_{YYA} = J_{YY} + J_{XYA} \cos 2 \phi_Z$$

$$J_{YY} = J_{Ayy} + J_{MXX} + J_{XYA}$$

$$J_{XYA} = \frac{1}{2} \left[J_{MYy} - J_{MXX} + \tan^2 \phi_X J_{MZZ} + \frac{J_{Oyy}}{\cos^2 \phi_X} \right]$$

$J_{AXX}, J_{Ayy}, J_{AZZ} \triangleq$ The polar moments of inertia of the inner gimbal about $\bar{l}_{XA}, \bar{l}_{YA}, \bar{l}_{ZA}$.

$J_{MXX}, J_{MYy}, J_{MZZ} \triangleq$ The polar moments of inertia of the middle gimbal about $\bar{l}_{XM}, \bar{l}_{YM}, \bar{l}_{ZM}$.

$J_{Oyy} \triangleq$ The polar moment of inertia of the outer gimbal about \bar{l}_{YO} .

$\phi_X, \phi_Y, \phi_Z \triangleq$ The gimbal angles of the X, Y and Z pivots.

$J_g \triangleq$ The gyro float moment of inertia about its output axis.

The derivation of the signal flow graph neglected all gimbal products of inertia of each gimbal. This approximation is valid since the mechanical design is symmetrical and all products of inertia should be small.

The characteristic equation of a three gimbal platform can be obtained from Figure 27 and is

$$\text{Eq. 16} \quad \Delta = \Delta_1 \Delta_2$$

where

$$\text{Eq. 17} \quad \Delta_Z = \left\{ \frac{H^2}{J_g p} + \frac{H G_Z}{J_g p^2} + p J_{AZZ} \right\}$$

Equation 17 is the characteristic equation of the Z loop considered as a single axis system and

Δ = The characteristic equation of the platform.

Δ_1 = The combined characteristic equation of the X and Y loop.

If the polar moments of inertia J_{AXX} and J_{AYY} of the inner gimbal are equal Δ_1 can be written as

$$\text{Eq. 18} \quad \Delta_1 = \Delta_X \Delta_Y$$

Where

$$\text{Eq. 19} \quad \Delta_X = \left\{ \frac{H^2}{J_g p} + \frac{H G_X}{J_g p^2} + p (J_{AXX} + J_{MXX}) \right\}$$

$$\text{Eq. 20} \quad \Delta_Y = \left\{ \frac{H^2}{J_g p} + \frac{H G_Y}{J_g p^2 \cos \phi_X} + p (J_{XX} + J_{XYA}) \right\}$$

Thus from equations 17, 19 and 20 it can be seen that the stability of the platform as a function of gimbal angle is a single axis loop study of the Y loop. Note the third term in equation 20 ($J_{XX} + J_{XYA}$) is a function of the angle ϕ_X the platform middle gimbal angle.

The ST124-M was designed with the constraint that

$$J_{AXX} = J_{AYY}$$

The question arises should secant ϕ_X gain compensation be used in the Y servo loop. If secant gain compensation were to be used, equation 20 would be written as

$$\text{Eq. 21 } \Delta_Y^{\text{Secant}} = \left\{ \frac{H^2}{J_g p} + \frac{H G_Y}{J_g p^2 \cos^2 \phi_X} + p (J_{XX} + J_{XYA}) \right\}$$

Assume the following numerical values for X or Y servo loop

$$H = 2 \times 10^6 \text{ gram cm}^2 \text{ sec}^{-1}$$

$$J_g = 1.17 \times 10^3 \text{ gram cm}^2$$

$$J_{XX} + J_{XYA} = \left\{ 4.2 + 1.7 \tan^2 \phi_X + \frac{0.84}{\cos^2 \phi_X} \right\} \times 10^6 \text{ gram cm}^2$$

$$G_X = G_Y = \left\{ 1.76 \times 10^9 \right\} \times$$

$$\left\{ \frac{\left(\frac{p}{8.5} + 1 \right) \left(\frac{p}{550} + 1 \right) \left[\left(\frac{p}{34.1} \right)^2 + 2(.68) \left(\frac{p}{34.1} \right) + 1 \right]}{\left(\frac{p}{2.13} + 1 \right) \left(\frac{p}{308} + 1 \right) \left[\left(\frac{p}{602} \right)^2 + 2(0.81) \left(\frac{p}{602} \right) + 1 \right]} \right\} \frac{\text{dyne cm}}{\text{rad}}$$

With the above numerical values substituted in equation 20, the Δ_Y characteristic equation has zeros listed in Table 1 as a function of ϕ_X . A plot of ξ the damping ratio for the low, middle and high frequency roots as a function of ϕ_X is shown in Figure 28.

When the above numerical values are substituted in equation 21, (the amplifier with secant compensation) the zeros for the Δ_Y^{Secant} characteristic equation are as shown in Table 2 and a plot of ξ the damping ratio for the three complex roots as a function of ϕ_X is shown in Figure 29.

The measure of stability is the magnitude of ζ of a complex pair of roots. A system is said to be more stable if its value of ζ is greater than that of another system. Comparing Figures 28 and 29, it can be said that the Y loop without secant compensation is somewhat more stable than the Y loop with secant compensation. Thus no attempt was made to use secant ϕ_X compensation in the Y servo loop.

TABLE NO. 1
ZEROS OF Δ_Y WITHOUT SECANT COMPENSATION

\emptyset	Real Root	Complex Root	ξ	Complex Root	ξ	Complex Root	ξ
0	$s + 8.90$	$s + 41.7 \pm j 23.9$	0.87	$s + 95.0 \pm j 106$.67	$s + 501 \pm j 301$	0.86
15	$s + 8.90$	$s + 41.5 \pm 24.3$	0.86	$s + 95.3 \pm j 105$.67	$s + 501 \pm j 300$	0.86
30	$s + 8.86$	$s + 41.2 \pm j 25.7$	0.85	$s + 95.8 \pm j 102$.68	$s + 501 \pm j 301$	0.86
45	$s + 8.80$	$s + 42.8 \pm j 28.6$	0.83	$s + 95.4 \pm j 86.7$.74	$s + 500 \pm j 304$	0.85
60	$s + 8.72$	$s + 42.3 \pm j 52$	0.63	$(s + 60.7)(s + 137)$	1.10	$s + 497 \pm j 311$	0.85
75	$s + 8.67$	$s + 11 \pm j 51.7$	0.21	$(s + 33.8)(s + 238)$	1.52	$s + 491 \pm j 327$	0.83

DAMPING RATIO (ζ) VERSUS θ_x FOR THE CHARACTERISTIC EQUATION

Equation 20
$$\Delta \gamma = \left(\frac{g^2}{v^2} + \frac{H \cdot g \cdot (1)}{g^2 \cos \theta_x} + P \cdot (1 + 0.188A^2) \right)$$

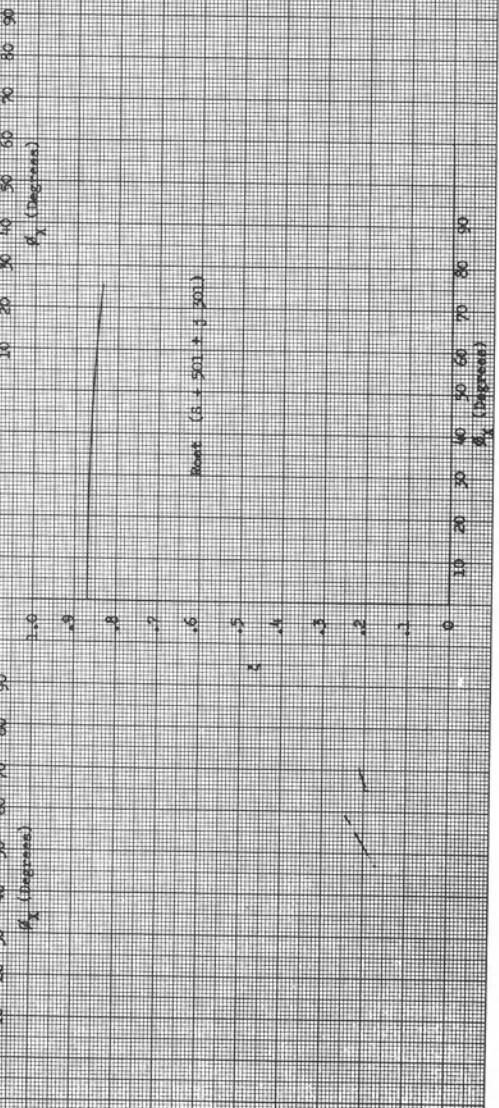
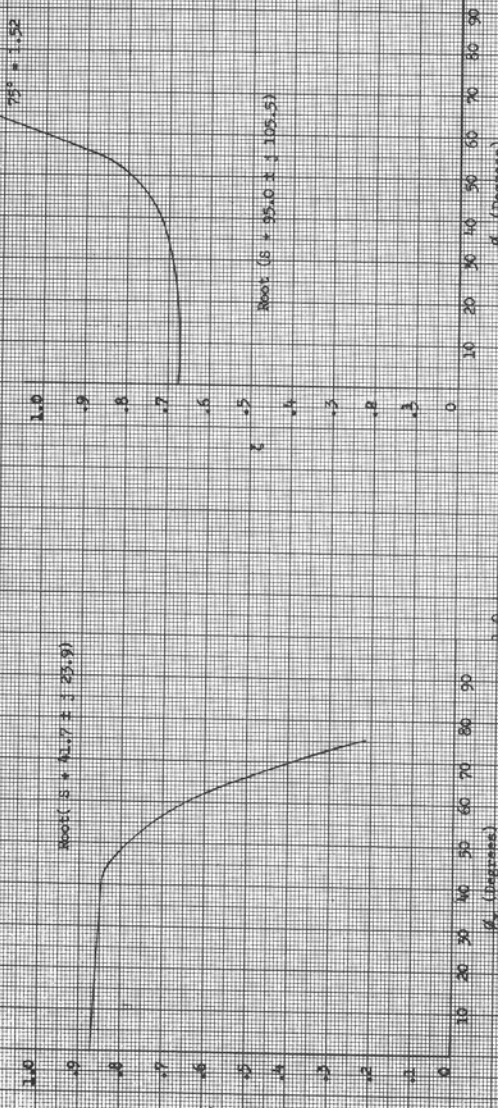


FIGURE 28

TABLE NO. 2
 ZEROS OF Δ_Y WITH SECANT COMPENSATION

ϕ	Real Root	Complex Root	ξ	Complex Root	ξ	Complex Root	ξ
0	$s + 8.9$	$s + 41.7 \pm j 23.9$.87	$s + 95.0 \pm j 106$.67	$s + 501 \pm j 301$.86
15	$s + 8.9$	$s + 39.5 \pm j 24.6$.85	$s + 96.3 \pm j 114$.65	$s + 502 \pm j 300$.86
30	$s + 8.8$	$s + 35.3 \pm j 25.8$.81	$s + 98 \pm j 136$.58	$s + 505 \pm j 294$.86
45	$s + 8.7$	$s + 31.5 \pm j 26.6$.76	$s + 96.8 \pm j 167$.50	$s + 510 \pm j 286$.87
60	$s + 8.6$	$s + 28.8 \pm j 27.1$.73	$s + 92 \pm j 200$.42	$s + 517 \pm j 275$.88
75	$s + 8.5$	$s + 27.3 \pm j 27.3$.71	$s + 85.6 \pm j 288$.35	$s + 525 \pm j 266$.89

DAMPING RATIO (ζ) VERSUS β_x FOR THE CHARACTERISTIC EQUATION

Equation 21
$$\Delta = \left(\frac{K^2}{g} \right) \left(\frac{H_0(X)}{g^2 \cos^2 \beta_x} + P \left(\frac{1}{X} + j \frac{Y_A}{X} \right) \right)$$

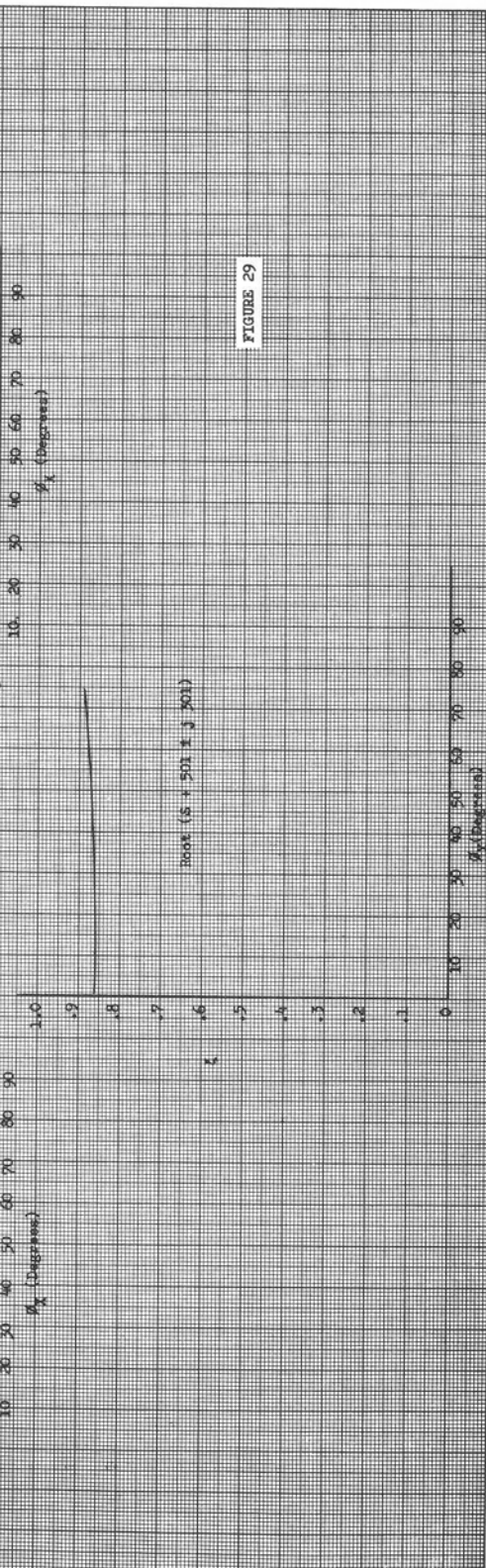
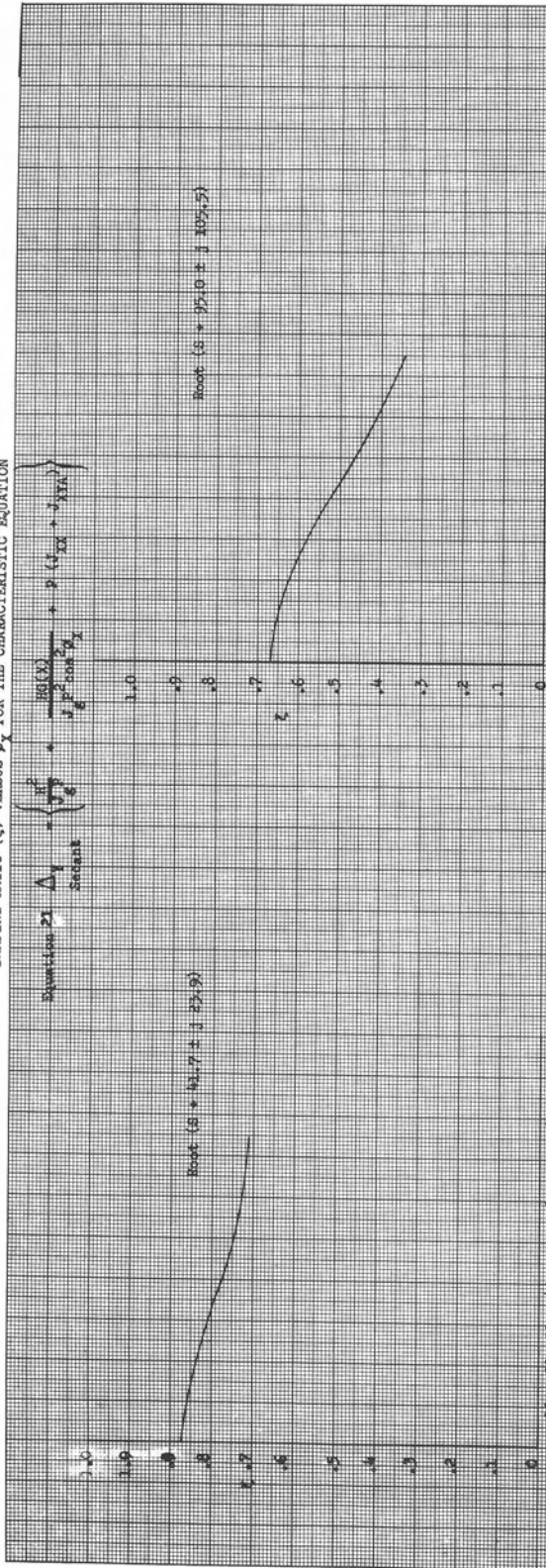


FIGURE 29

SECTION 6.0

THE CONING OR RECTIFICATION DRIFT OF A THREE GIMBAL PLATFORM

A three gimbal platform with a displaced middle pivot and ideal gyros is subject to the rectification drift problem.

A vehicle rotation about the pitch axis with the middle gimbal displaced at an angle ϕ_x will produce an angular rate on the inner gimbal. This type of angular vibration is usually in a frequency range where the servo loop cannot compensate for the inner gimbal motion. It is this type motion that will generate a rectified moment about the output axis of the gyro, thus causing the inner gimbal to have a steady state drift.

The **rectified** moment equation can be expressed as

$$\text{Eq. 22} \quad M_R = H A W_{I-SRA}$$

where

H = the wheel angular momentum

A = the output axis displacement

W_{I-SRA} = the angular velocity of the gyro case about its spin reference axis.

From the orientation of the gyros in Figure 2, the rectified moments can be expressed as

$$\text{Eq. 23} \quad M_{RX} = -H \left\{ \frac{H W_{IAXA}}{J_g p^2} \right\} \left\{ W_{IAZA} \right\}$$

$$\text{Eq. 24} \quad M_{RY} = -H \left\{ \frac{H W_{IAYA}}{J_g p^2} \right\} \left\{ W_{IAZA} \right\}$$

$$\text{Eq. 25} \quad M_{RZ} = -H \left\{ \frac{H W_{IAZA}}{J_g p^2} \right\} \left\{ -W_{IAXA} \right\}$$

It can be seen from equations 23, 24 and 25 that if rectified drift is to occur a rate component along the Z axis of the inner gimbal must be present. However, if one assumes the platform Z pivot is frictionless any base motion must be lost in this pivot and W_{IAZA} is zero. Thus all three rectification moments must be zero regardless of the angle ϕ_X .

It can be said that ideally no rectification moment will be obtained if the three output axis of the gyros are mounted perpendicular to the inner gimbal pivot. Thus there are two reasons for the gyro orientation in Figure 2, one to minimize the anisoelastic drift and ~~the other~~ to eliminate the rectification drift.

It can be shown with the friction levels present in the ST124-M and assuming a white noise power spectral density at $\phi_X = 45^\circ$ the rectification moment due to pivot friction will be less than 0.16 dyne cm, which is quite acceptable. There will be negligible rectification from linear vibration and gimbal pendulousity since the platform gimbals are balanced to better than 25 gram cm.

In summary the ST124-M angular base rotation rectification drift problem can be neglected.

SECTION 7.0

A PHYSICAL DESCRIPTION OF THE ST124-M PLATFORM

Outline drawings of the three and four gimbal platforms are shown in Figures 30 and 31. The platform mounts solid to the vehicle on three accurately machined mounting surfaces which will align the platform base to the launch vehicle coordinates.

The platform is designed to operate in a hard vacuum. The spherical section covers are sealed to the platform base with a full volume "O" ring seal and a critical orifice in the cover provides a discharge path for the gas bearing exhaust. A nitrogen atmosphere of 12 psia is maintained inside the platform in vacuum while at sea level the inside of the platform is pressurized to 3 psig above atmospheric pressure. The covers also contain a path for fluid to circulate between the walls, and this heat exchanger will condition the temperature of the inner gimbal with the aid of internal gas blowers to provide an even temperature distribution throughout the platform.

All gimbals, the base and trunnions are fabricated from beryllium material. Beryllium was selected, for its strength to weight ratio, stability after machining and its heat transfer properties. The inner gimbal will be machined so that the accelerometer will mount in an orthogonal triad within ± 5 arc seconds. The other gimbals and base will be spherical or cylindrical sections with an orthogonality between pivots of ± 5 arc seconds on any gimbal. The spherical or cylindrical sections minimize anisoelastic moments of the gimbals, provide symmetrical moments of inertia for the servo loops and an optimum shape for mechanical gimbal stability. The inner, middle and outer gimbals are shown in Figure 32 while the redundant gimbal and frame are shown in Figure 33.

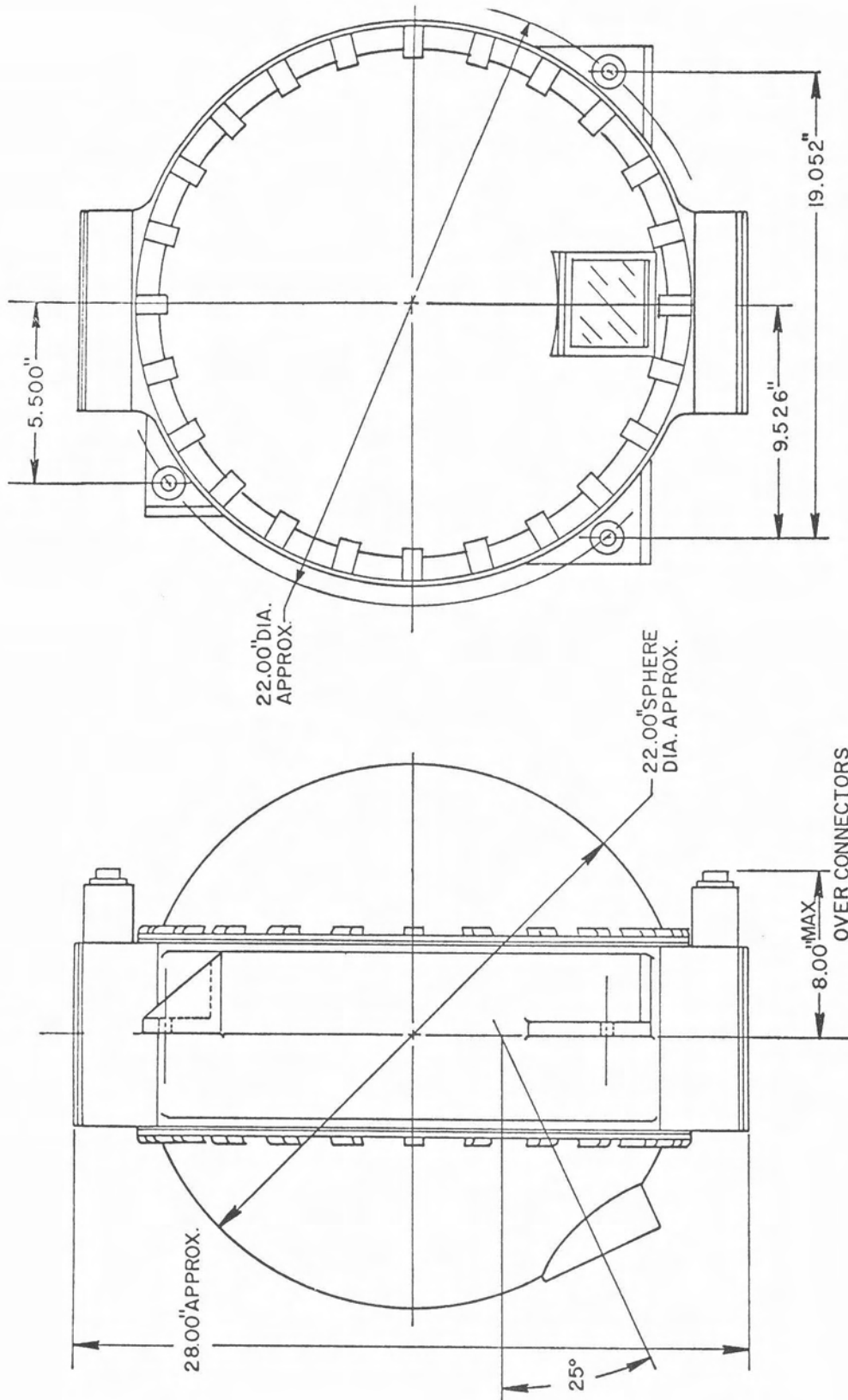


FIGURE 30
 ST124-M THREE GIMBAL PLATFORM

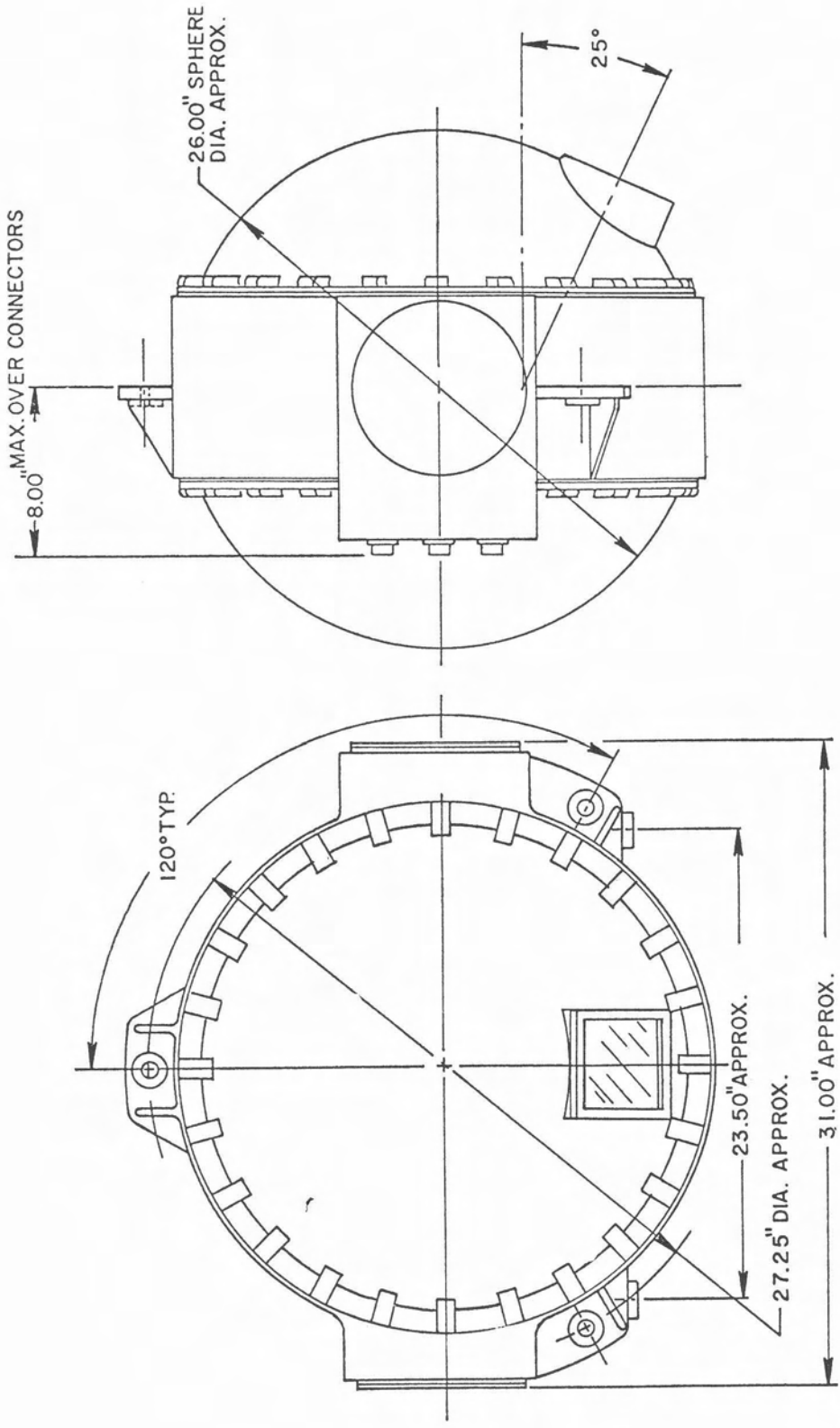


FIGURE 31
 ST124-M FOUR GIMBAL PLATFORM

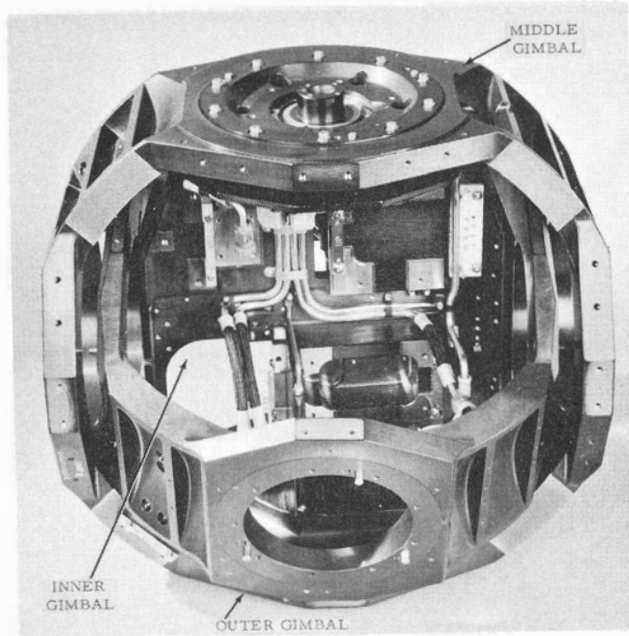


FIGURE 32
INNER, MIDDLE AND OUTER GIMBALS

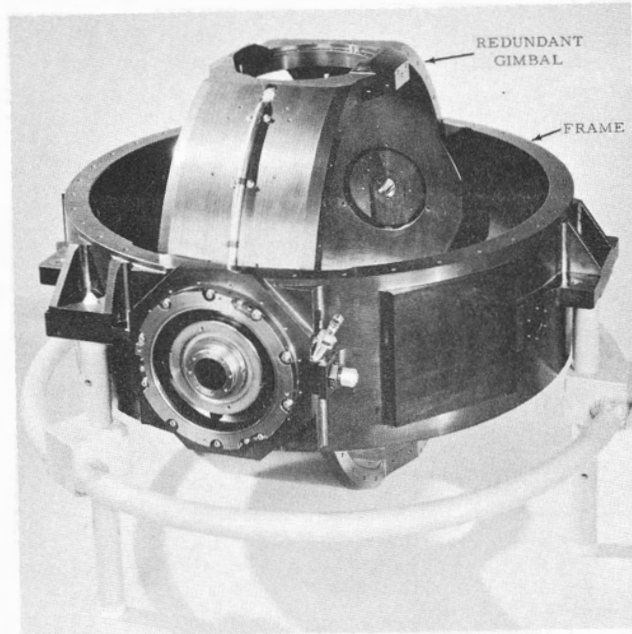


FIGURE 33
REDUNDANT GIMBAL AND FRAME

The gimbal load bearings are a preloaded pair of bearings on one side and a gothic arch type bearing on the other side of the gimbal. Thus the bearing preload is not obtained by stressing the gimbal and more accurate preloads are obtained for each gimbal. The platform resolvers are assembled in separate housings with their own bearings to obtain the best possible machining concentricities on the rotor and stator of the resolver to reduce the one cycle error. The complete assembly is coupled to the pivot with an extremely stiff diaphragm. With reasonable alignment between the two shafts it can be shown that the diaphragm does not introduce the Hook's joint type of errors. This type of construction enables replacement of the gimbal sensors without complete disassembly of the platform or removal of the load bearings.

The pivots contain a gas annulus with "O" ring seals to transfer the gas from one gimbal to another. The pivot leakage is negligible and the air seals contribute a friction torque of less than 5 in oz. A flex cable joint is used on the X pivot since its motion is limited. This flex joint has 180 circuits and contributes less than 5 in oz. when the gimbal is deflected 60 degrees.

A structural resonant frequency of 120 cps is obtained on the inner gimbal which is due to the stiffness of the gimbal rings. There is a secondary resonant frequency of the inner gimbal at 280 cps which is obtained from the bearings and trunnions. Above 280 cps the inner gimbal attenuates the base vibration input and provides a smooth frame. The 120 cps is sufficiently removed from all vehicle resonant frequencies.

The ST124-M three and four gimbal platforms weigh 107 and 146 pounds respectively and require 15 psig (referenced to the inside platform chamber) 0.5 Standard Cubic Feet per Minute of dry gaseous nitrogen.

Two views of the platform without covers are shown in Figures 34 and 35. Figure 34 shows an assembled platform with covers removed while Figure 35 shows a view of the fixed and movable prism.

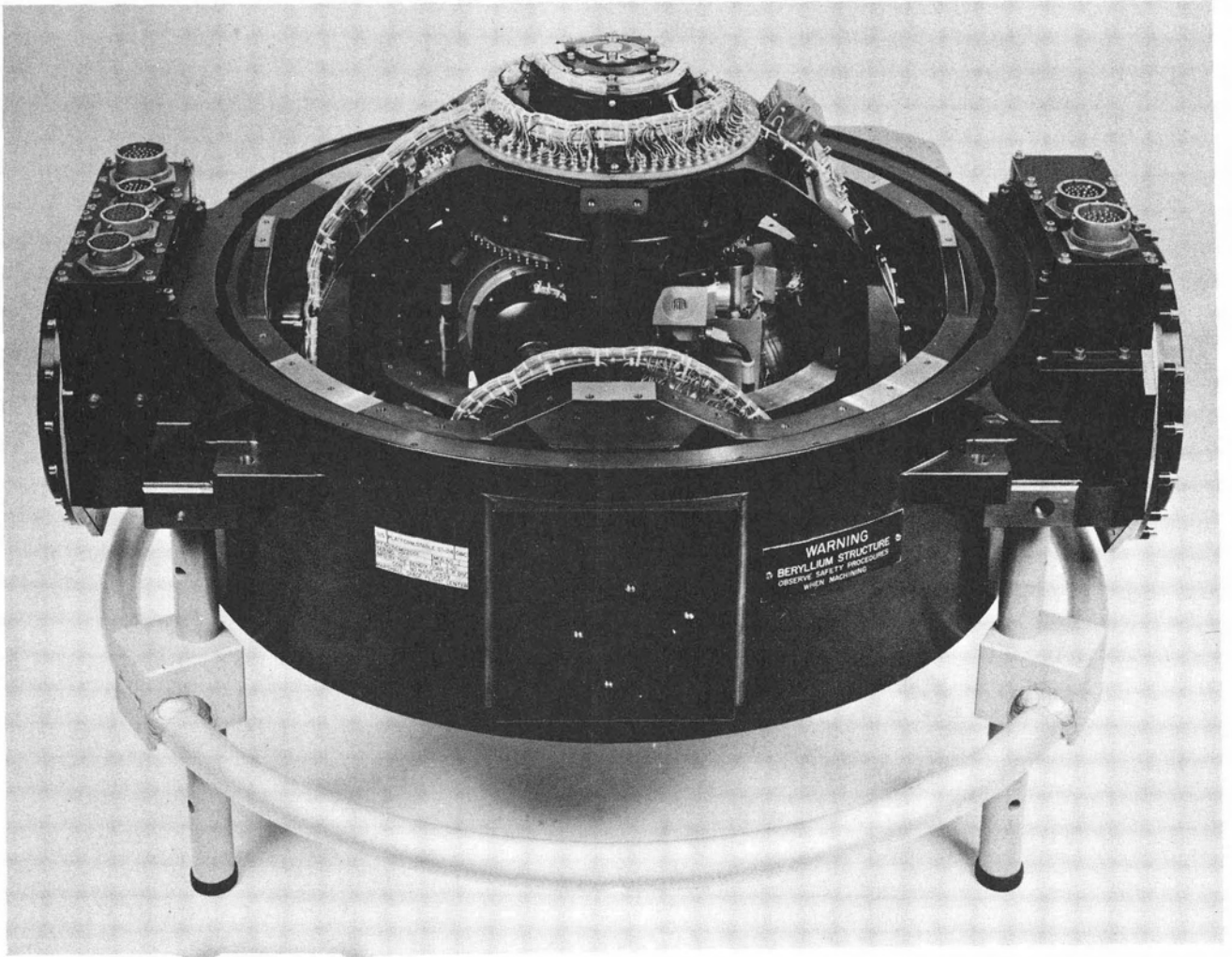


FIGURE 34
ST-124 PLATFORM WITH COVERS REMOVED

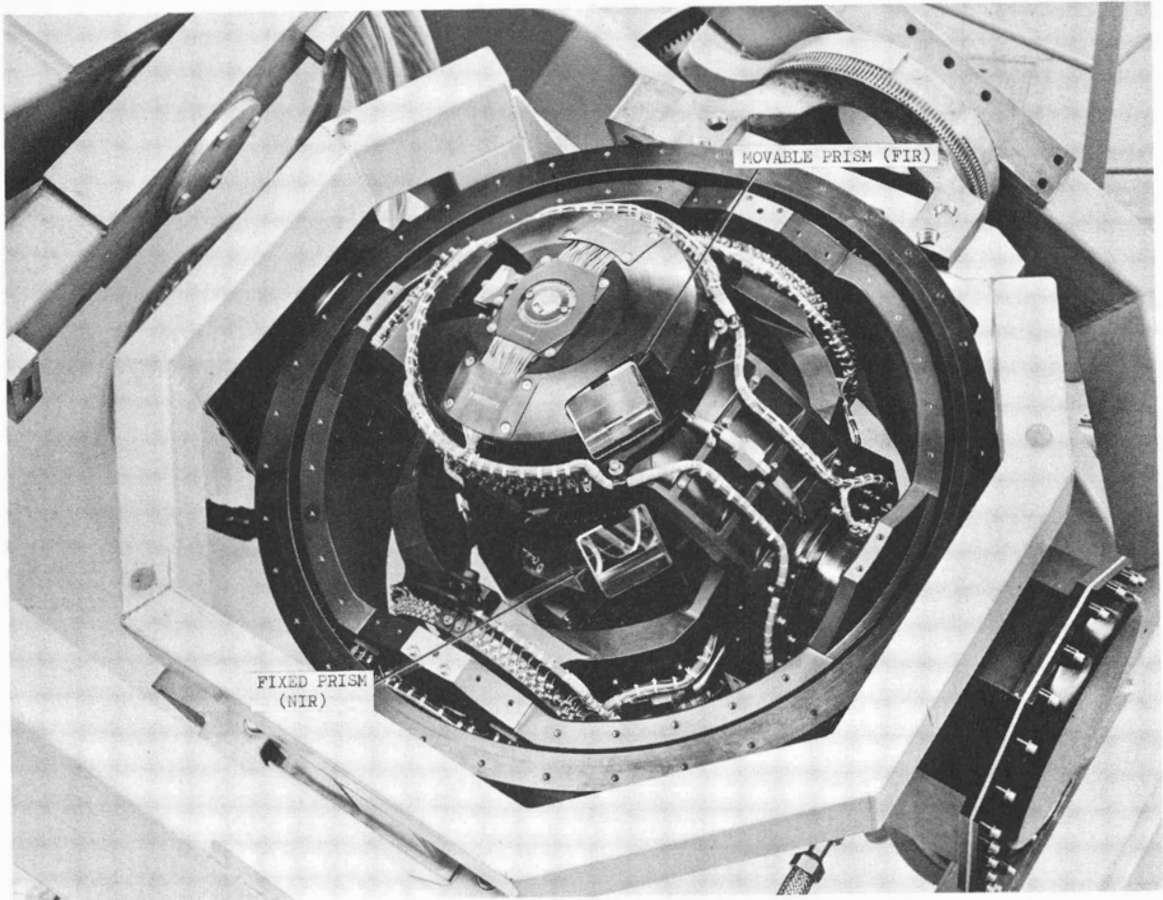


FIGURE 35
FIXED AND MOVABLE PRISM

SECTION 8.0

THE PLATFORM SERVO AMPLIFIER ASSEMBLY

The platform servo amplifier assembly will contain the electronics other than those located in the platform, required for the platform axis and the accelerometer stabilization. The following is a list of components for the ST124-M four gimbal platform electronics assembly.

1. Three gyro servo amplifier cards
2. Three gimbal torquer power stages
3. One redundant gimbal servo amplifier card
4. One redundant gimbal torquer power stage
5. Three accelerometer servo amplifier cards
6. Three accelerometer torquer power stages
7. One 4.8 KC voltage amplifier card
8. An automatic checkout circuit selector module
9. One current transformer assembly for monitoring gyro wheel currents
10. Two relay card assemblies
11. One elapsed time indicator
12. Three power switching relays
13. Eight electrical connectors
14. One 400 cps keying transformer
15. One temperature sensor.

The majority of the items listed will be plug-in modules. The assembly for the three gimbal platform will be identical except that items 3 and 4 will be deleted.

Components or modules requiring pressurization will be protected by encapsulation. Internal heat sources will be heat-sunked to the main casting and cooling will be realized by conduction into the temperature-controlled mounting panels of the instrument unit. For system flight evaluation, critical control signals are conditioned and supplied to telemetering from this assembly.

The platform electronics assembly will be a cast magnesium structure and will be mounted to the vehicle frame with pads which extend out from the box structure. The box will have sheet metal covers on three sides. A gasket will be used to provide a dust-tight seal. Internally, the box will contain a cast magnesium deck for mounting electronic components and a grooved rack for mounting printed circuit modules. The assembly will weigh 42 pounds.

A gyro servo amplifier card is shown in Figure 36 while the torquer power stage is shown in Figure 37. Figure 38 shows the hardware which comprises a gimbal servo loop and Figure 39 is a view of the platform electronic assembly.

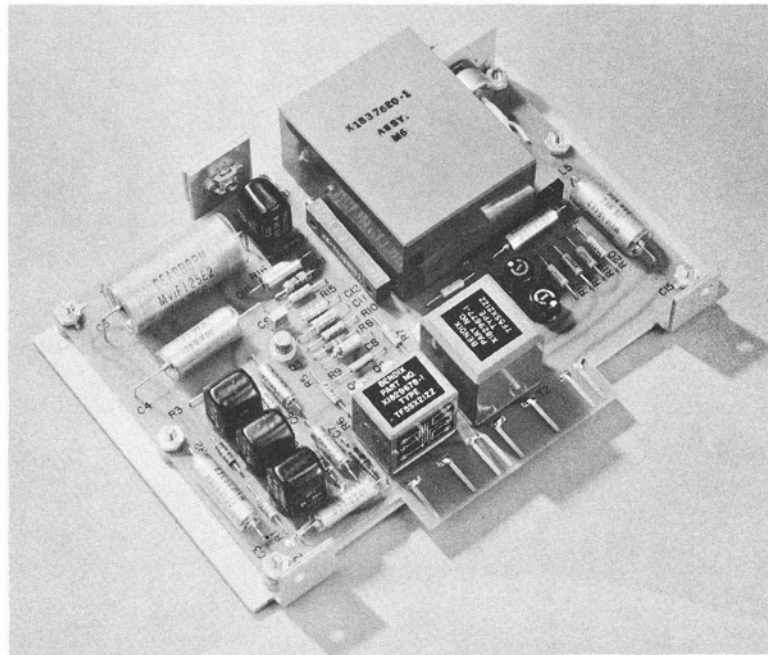


FIGURE 36
SERVO AMPLIFIER CARD

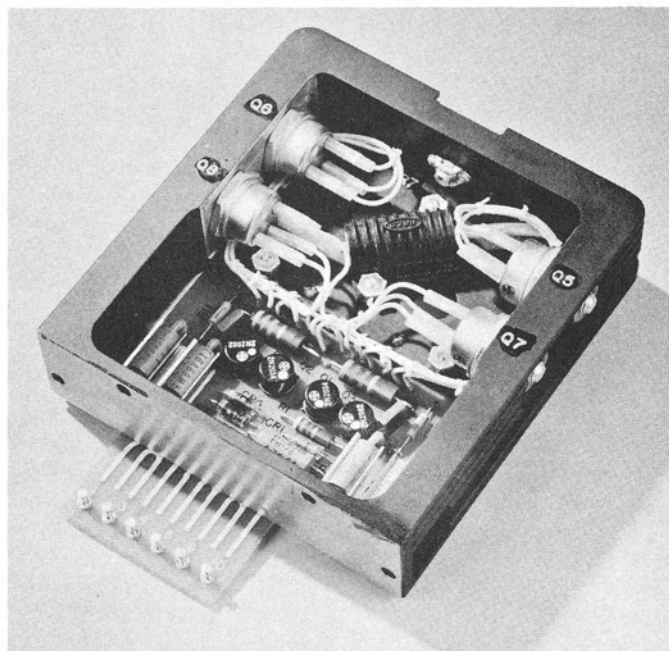


FIGURE 37
TORQUER POWER STAGE

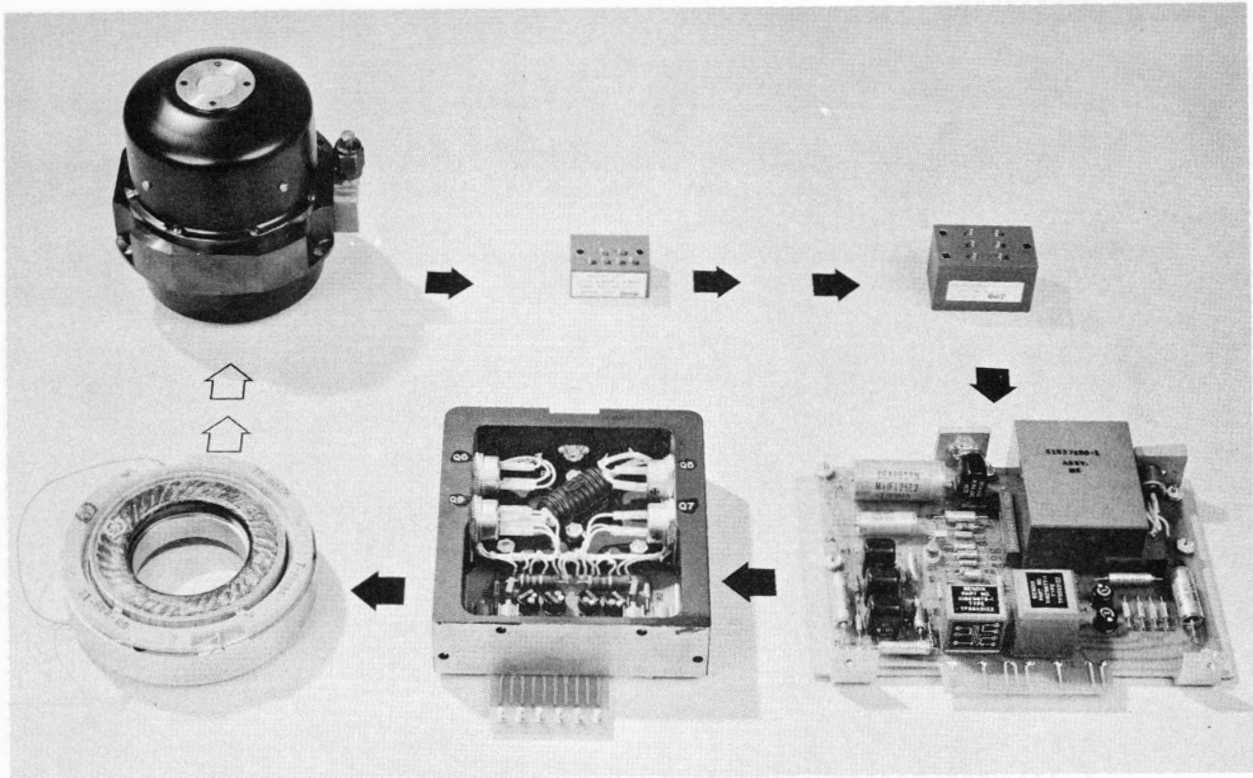


FIGURE 38
GIMBAL SERVO LOOP

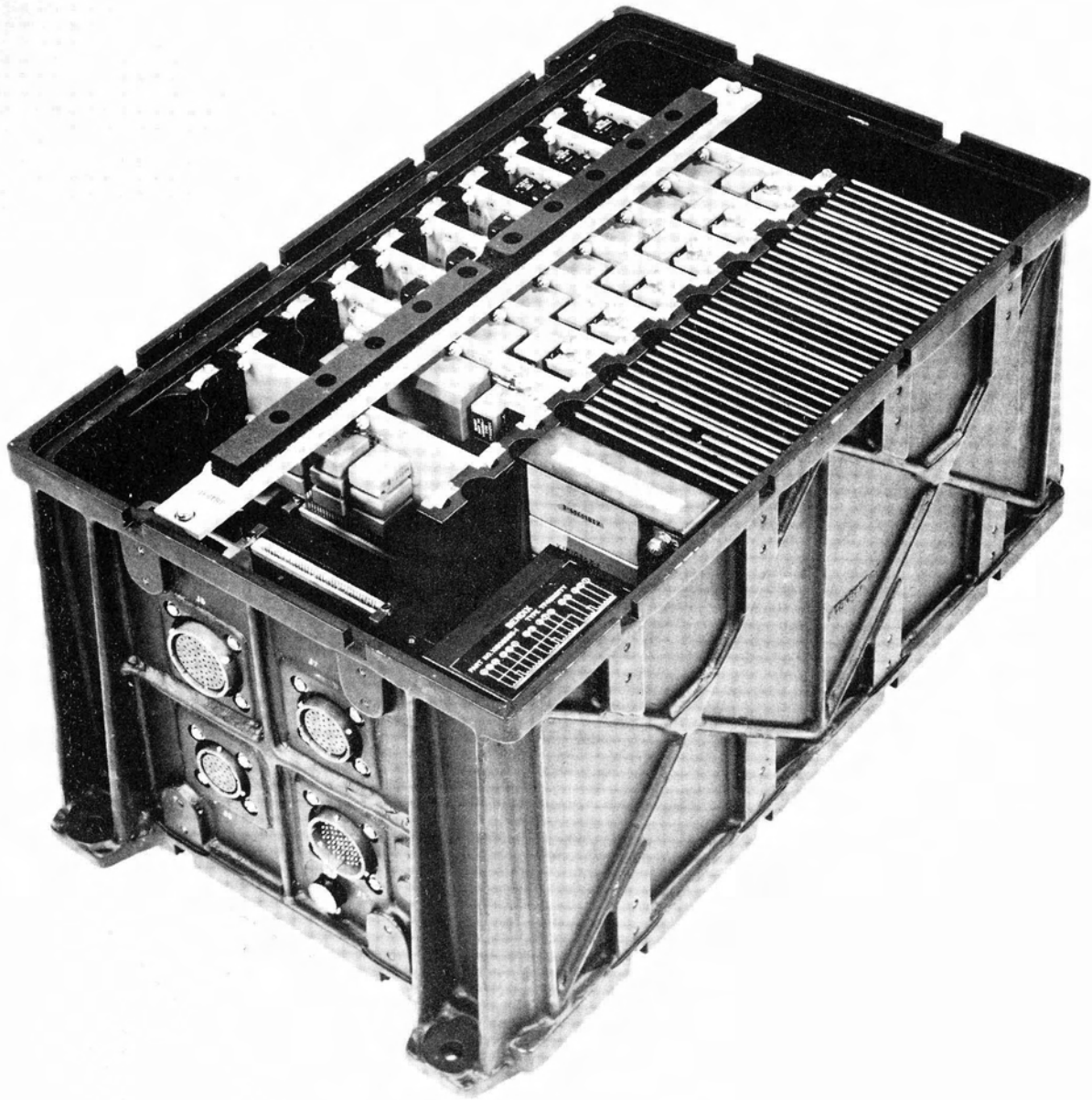


FIGURE 39
PLATFORM SERVO AMPLIFIER ASSEMBLY

SECTION 9.0

THE A.C. POWER SUPPLY

The platform A.C. power supply assembly furnishes the power required to run the gyro wheels, excitation for the platform gimbal synchros, and frequency sources for the resolver chain excitation and servo carrier. All frequencies are derived from a crystal oscillator and are accurate to 25 parts per million. The A.C. power supply box will be cast of magnesium and will have a light gauge sheet metal cover, gasket sealed for dust protection. Modular potted construction will be used throughout. Motherboard printed circuits will be used and the only harness wiring will encompass only the electrical connectors. The weight of the assembly is 32 pounds.

The following outputs are generated in the A.C. power supply:

1. 26 volt, 3 phase, 400 cps \pm 0.01 cps
2. 20 volt, 4.8 KC \pm .12 cps square wave
3. 20 volt, 1.6 KC \pm .04 cps square wave
4. 20 volt, 1.92 KC \pm 0.48 cps square wave

The A.C. power supply is rated at 250 VA with a conversion efficiency of 70% at full load. The harmonic distortion of the 400 cps is 1.5%. A redundancy is provided in the A.C. power supply for all circuits including the crystal oscillator.

BIBLIOGRAPHY

- Gille, J.C., Pelegrin, M.J., Decaulne, P., Feedback Control Systems Analysis, Synthesis and Design, McGraw Hill, 1959.
- Savet, P.H., Gyroscopes, Theory and Design, McGraw Hill, 1961.
- Thomson, W. T., Introduction to Space Dynamics, John Wiley, August, 1963.